METHANE FLUX FROM RECENTLY EXPOSED SUBGLACIAL SEDIMENTS, ROBERTSON GLACIER, CANADA

by

Terra Marie Spotts

A thesis submitted in partial fulfillment
of the requirements for the degree

of

Master of Science

in

Earth Sciences

MONTANA STATE UNIVERSITY
Bozeman, Montana

April 2014

ACKNOWLEDGEMENTS

I would like to extend a sincere thank you to my advisor, Dr. Mark Skidmore for his support and the opportunity to be a part of this research. A kind thanks also to Dr. Jim Schmitt for reminding me of the big picture, Dr. John Dore for his guidance, advice, crash course in physical chemistry and the stimulating football conversations, and Dr. Eric Boyd for his quality input, contributions and thoughts regarding this research. To Ryan and Lena, thank you for keeping the long days in the field and lab lighthearted and fun. Thank you to my family and friends for your endless support and patience and to my primary sounding board, thank you Edward.

TABLE OF CONTENTS

1. INTRODUCTION AND LITERATURE REVIEW 1

General Overview 1
Literature Review 2
Global Methane Budget 2
Microbially Controlled Methane Cycling 6
Glacial Systems 8
Broader Implications 12
Research Objectives 13

2. METHODS 14

Study Site 14
Static Gas Flux Chambers 17
GFC Design and Deployment 17
GFC Gas Sample Collection 21
Ambient Sample Collection 22
Gas Analyte Measurements 22
Gas Standards 23
GFC Gas Flux Calculations 23
Vertical Sediment Cores 26
Sediment Core Collection and Sample Preparation 27
Sediment Gas Sampling 28
Gas Chromatography 29
Glass, Metal and Plasticware Preparation 29
Sediment Characterization 30
Gas Concentration Calculations 31

3. RESULTS 33

Static Gas Flux Chambers 33
Methane Concentration Statistical Analysis 34
Trends in Gas Analyte Fluxes 34
Methane Flux Spatial and Temporal Statistical Analysis 42
Methane Flux in GFC Depth Trio 45
Regression Analysis: Temperature, CO and CO_2 Fluxes 45
Vertical Sediment Core Profiles 50
Sediment Core Gas Profiles 50
Sediment Core Porosity, Porewater and POC 51

TABLE OF CONTENTS - CONTINUED

Statistical Analysis of Physical Parameter Correlation with Methane Concentration 56
Diffusive Methane Fluxes 59

4. DISCUSSION 63

Methane Fluxes: Temporal and Spatial Variability 64
Surface Methane Flux 64
Subsurface Methane Flux 65
CO Surface Flux 66
Heterogeneous Concentrations of Gases throughout Vertical Sediment Core Profiles 67
Diffusivity of Methane, CO and CO_2 through Vertical Core Profile 72
Comparison of RG Methane Fluxes to Other Glaciated Environments 74
Future Research 76
Conclusion 76

REFERENCES CITED 78

APPENDICES 86

APPENDIX A: Gas Chromatograph Schematics 87
APPENDIX B: CH_4, CO_2 and CO Flux Values 89

LIST OF TABLES

Table Page

1.1. Global Methane Source and Sink Strength and $\delta^{13}C$ Values 5

2.1. CH_4, CO_2, H_2 and CO Bunsen Coefficients 32

3.1. Methane Concentration Statistical Parameters 35

3.2. Average Concentration of CH_4, CO, H_2 and CO_2 for Each Core at Depth.....55

3.3. Statistical Analysis Summary for Cores A-D 57

3.4. Diffusive Gas Fluxes Based on Sediment Water Saturation 61

LIST OF FIGURES

Figure Page

1.1. Global Methane Sources and Sinks 4

1.2. Sediment Exposure at a Retreating Glacier 10

2.1. Robertson Glacier Location Maps 15

2.2. Gas Flux Chamber Locations 16

2.3. Schematic and Photos of Gas Flux Chambers 20

2.4. Second Order Polynomial Curve for Gas Flux Chamber Rates of Change: Positive and Negative Fluxes 24

2.5. Diagram of Relative Location of Sediment Core Collection Sites 27

3.1. Matrix Diagram of CH_4 Flux Magnitudes for Each GFC 36

3.2. Matrix Diagram of CO_2 Flux Magnitudes for Each GFC 37

3.3. Matrix Diagram of CO Flux Magnitudes for Each GFC 38

3.4. Ratio of Positive to Negative Fluxes by GFC for CO, CO_2 and CH_4 39

3.5. Spatial Distribution and Magnitudes of Methane Fluxes for Each Sampling Period 40

3.6. Sediment Volumetric Water Content and Temperature with Distance from Glacier Terminus 41

3.7. Mean Methane Flux of All GFCs for Each Sampling Period 43

3.8. Mean Methane Flux for Each GFC for Collective Sampling Period 44

3.9. Cumulative Methane Fluxes for Each GFC 44

3.10. Mean Methane Flux at Depth for Each Sampling Location 46

LIST OF FIGURES - CONTINUED

Figure Page

3.11. Methane Flux vs Sediment Temperature for Each GFC 47

3.12. Methane Flux vs CO and CO_2 Fluxes for Each GFC 49

3.13. Vertical Sediment Profiles for 2011 Cores: A and B.....53

3.14. Vertical Sediment Profiles for 2012 Cores: C and D.....54

3.15. Linear Regression Plots for Core Gas Analytes, POC, and Porewater.....58

3.16. Diffusivity Curves based on Percent Water Saturation and Porosity 62

4.1. Metabolic Pathways for Methane Production.....69

4.2. Methane Fluxes Reported in Comparable Environments to RG.....75

ABSTRACT

Methane is over 20 times more effective than CO_2 as a greenhouse gas. Thus, its atmospheric concentration and the processes controlling it are important components of the global climate system. Recent research has shown methanogenesis in subglacial sediments. However, the net contribution from subglacial systems to the global methane budget is poorly understood due to a dearth of empirical data.

Using measurements via the static chamber method, the flux of methane from recently exposed subglacial sediments at Robertson Glacier, Canadian Rockies was quantified. Methane concentrations were measured from surface gas flux chambers in transects both parallel and perpendicular to the glacier terminus. Over 300 measurements were made during the 2012 melt season (July to September) and used to determine both spatial and temporal variability in the gas fluxes. The chamber farthest from the glacier terminus, approximately 50 m down valley, had an average flux close to zero whereas the chambers nearest the terminus had the highest average fluxes. The average methane efflux from the sediment surface to atmosphere was 0.22 $\mu mol\ m^{-2}\ d^{-1}$. The highest methane efflux during the season, 11.0 $\mu mol\ m^{-2}\ d^{-1}$, was measured in close proximity to the glacier terminus.

Shallow sediment cores were collected adjacent to the static chambers and vertical gas concentration profiles were measured from the cores. Within the profiles, methane concentrations were greater than atmospheric concentrations at all depths. Additionally, CO_2, CO and H_2 gas concentrations were analyzed in the cores to evaluate potential microbial metabolic pathways of methane production.

Previous studies on methane fluxes from glacial sediments in Greenland and the Swiss Alps used single time point flux measurements during a melt season from multiple locations. This study concludes that such point measurements are unlikely representative for determining a net seasonal flux as they do not consider temporal variability. There was a two order of magnitude difference between the annual source contribution of methane based on the average melt season flux and the highest measured surface flux. This indicates that single sampling periods may significantly over or underestimate the net seasonal flux of methane from recently exposed glacial sediments to the atmosphere.

CHAPTER 1 – INTRODUCTION AND LITERATURE REVIEW

1.1 General Overview

The global atmospheric methane mixing ratio is 1.79 ppmv (Dlugokencky et al., 2011) making it Earth's most abundant atmospheric hydrocarbon gas. The current global methane budget is 500-600 Tg (1 Tg = 1.0 x 10^6 metric tons) per year, however, this budget does not include the subglacial environment as a contributing source. The current extent of ice cover is approximately 11% of Earth's surface and up to 30% and 100% of the Earth's surface was ice covered during Pleistocene glaciations and the Neoproterozoic era (Kirschivink, 1992), respectively. If indeed the subglacial environment is an active biome, the flux of methane from subglacial sediments during deglaciation may prove to be of significance to the global methane budget (Wadham et al., 2012).

Research from Robertson Glacier (RG) in the Canadian Rockies (Boyd et al., 2010), east Greenland (Barcena et al., 2010) and the Swiss Alps (Nauer et al., 2012) has demonstrated the presence of excess methane in subglacial sediments at the terminus of retreating ice masses. However, it is unknown whether the methane flux at RG is *a)* positive, a net source, or negative, a net sink during the ablation season and *b)* seasonally and spatially variable due to changing conditions in the glacial sediments.

Here we present a systematic and comprehensive study of the spatial and seasonal flux of methane from recently exposed glacial sediments demonstrated using measurements via the static chamber method and vertical sediment core profiles. RG, an

alpine glacier in the Canadian Rockies, was chosen as the study site because of the significant amount of prior research conducted there, including bedrock geology mapping (McMechan, 1998), analysis of runoff composition and mineral weathering (Sharp et al., 2002; Mitchell et al., 2013) and microbial community investigations (Boyd et al., 2010; Boyd et al., 2011; Hamilton et al., 2013). Following is a brief review of global methane cycling and the subglacial environment.

1.2 Literature Review

1.2.1 Global Methane Budget

The current methane budget from global sources is 500-600 Tg per year (Dlugokencky et al., 2011; Aronson et al., 2013) with the majority of methane production and consumption driven by microbial activity (Conrad, 2009). Methane is known to be at least 20 times more effective as a greenhouse gas than CO_2, on a molar basis, rendering a thorough understanding of its global sources and sinks valuable.

Recently, new methane sources have been documented and known sources, that are not well quantified (Wolff and Spahni, 2007; Aronson et al., 2013), vary in reported strength (IPCC, 2007; Dlugokencky et al., 2011). Natural sources of methane, including wetlands, termites, and oceans, account for around 32% of the source contribution while anthropogenic sources account for the other 68% (see Figure 1.1). Recently, thermokarst lakes and shallow marine hydrates have also been recognized as potentially significant sources of atmospheric methane; contributing 3.7 Tg yr^{-1} (Walter et al., 2006) and 1.5 Tg

per Arctic summer (~100 days[1]) (Shakhova et al., 2010), respectively, which would increase the source contribution to the total budget. Methane is short lived in the atmosphere with a residence time around 9 years due to efficient removal by reactions with hydroxyl free radicals (OH^-) (Wolff and Spahni, 2007; Dlugokencky et al., 2011) which accounts for 89% of the methane sink globally (Figure 1.1). The soil sink is largely due to methanotrophs which oxidize methane accounting for up to 10% of the total methane sink (Aronson et al., 2013 and references within).

The atmospheric methane concentration has increased over time due to anthropogenic influences (Allan et al., 2001; Breas et al., 2002; Dlugokencky et al., 2011) as evidenced by the change in $\delta^{13}C_{CH4}$ value from -49‰ to -47‰ (Wolff and Spahni, 2007). Anthropogenic sources of methane such as biomass burning and coal mining tend to have more positive $\delta^{13}C_{CH4}$ values as compared to natural sources of methane such as wetlands and termites (Table 1.1). Based on ice core data from Greenland and Antarctica, which reveals the changing conditions of the atmosphere over time (Raynaud et al., 1992; Stauffer, 2000; Souchez et al., 2006; Melton et al., 2011); atmospheric methane concentrations have varied between 350 to 700 ppbv during glacial-interglacial periods within the past 650 ka (Wolff and Spahni, 2007). However, the global atmospheric methane concentration has increased since pre-industrial time (mid-18th century) from ~0.7 ppmv to, its present day value, 1.79 ppmv (Dlugokencky et al., 2011) which is well outside the range of concentrations from the past 650 ka.

[1] Not on an annual basis because the methane emissions during fall may be affected by water column mixing and winter emissions may be affected by ice coverage, flaw polynyas and ice breakup where these emission values are not yet known (Shakhova et al., 2010).

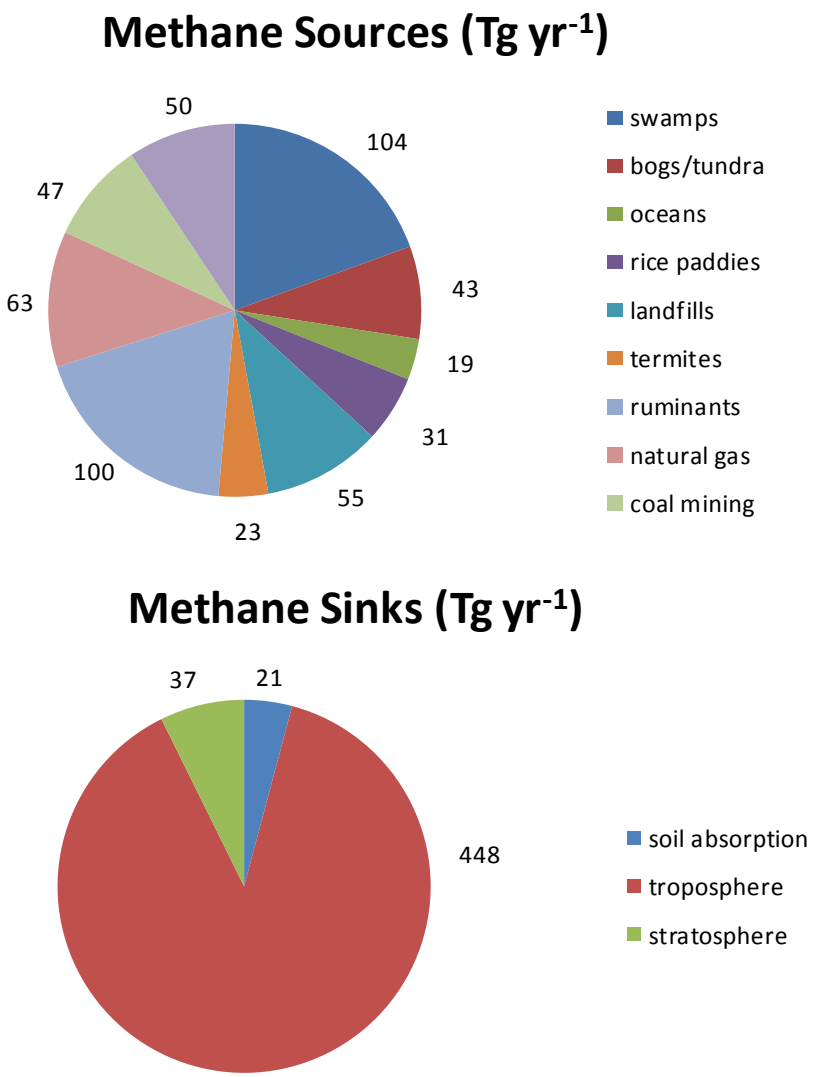

Figure 1.1: Global methane sources and sinks. Values are reported in Tg yr^{-1}. Based on data from Dlugokencky et al. (2011).

Table 1.1: Global methane source and sink strengths and $\delta^{13}C_{CH4}$ value for each source. Data from Dlugokencky et al. (2011), IPCC (2007) and references within.

Methane Sources	*Tg yr^{-1} Dlugokencky et al. (2011)*	*Tg yr^{-1} IPCC (2007)*	*$\delta^{13}C$ (‰)[c]*	*$\delta^{13}C$ (‰)[d]*
Natural				
Wetlands (total)	147	100-231	n.d.	-58
bogs/tundra	43	n.d.	-55	n.d.
swamps	104	n.d.	-65	n.d.
Geological	n.d.[e]	4-14	n.d.	-40
Hydrates	n.d.	4-5	n.d.	-60
Oceans	19	4-15	-58[a]	-60
Termites	23	20-29	-49, -70[b]	-70
Wild ruminants	5-10	15	n.d.	-60
Wildfires	n.d.	2-5	n.d.	-25
Sub total	*194-199*	*149-314*		
Anthropogenic				
Landfills	55	35-69	-53	-55
Rice paddies	31	31-83	n.d.	-63
Ruminants	90	76-92	-62	-60
Natural gas/oil	63	52-68	n.d.	-44
Coal mining	47	30-46	-35	-37
Biomass burning	50	14-88	-17, -26[b]	-25
Sub total	*336*	*238-446*		
Total	*530-535*	*387-760*		
Methane Sinks				
Troposphere	448	428-511		
Stratosphere	37	30-45		
Soil	21	26-34		
Total	*506*	*492-581*		

[a] from Whiticar and Schaefer (2007)
[b] first value is for C4 vegetation and second value is for C3 vegetation
[c] from Dlugokencky et al. (2011)
[d] from IPCC (2007)
[e] n.d. is no data

1.2.2 Microbially Controlled Methane Cycling

Microbes have been recognized as important contributors to the biogeochemical cycling of carbon, nitrogen, sulfur, iron and phosphorus and they have the ability to regulate atmospheric constituents such as O_2, CO_2 and CH_4 through interactions with mineral and rock substrates (Ehrlich, 1998). Microbial impacts on geochemical cycling have been investigated in sedimentary environments (Conrad, 1995) and subglacial sediments (Skidmore et al., 2005; Montross et al., 2013).

Methane on Earth is of two origins, either biotic or abiotic, with the biogenic source contributing the majority to atmospheric concentrations (Conrad, 1996). Methanogens are responsible for at least 70% of the total methane source (Dlugokencky et al., 2011). Several of the major atmospheric sources (i.e. termites, ruminants, wetlands, rice paddies, landfills) are the result of methanogenic activity where methanogens, strict anaerobes, reside in these anoxic environments and utilize the substrates present to produce methane. There are two general metabolic pathways of microbial methane production 1) hydrogenotrophic (reduction of CO_2 with H_2) or 2) acetoclastic (acetate fermentation):

1) $CO_2 + 4H_2 \rightarrow CH_4 + 2H_2O$

2) $CH_3COOH \rightarrow CH_4 + CO_2$

In general, methane production depends on temperature, water table level (i.e. degree of saturation) which creates anoxic conditions, organic carbon (OC) content and pH

(Kotsyurbenko et al., 2004). Possible controls on the predominant metabolic pathway, CO_2 reduction or acetate fermentation, may be sediment temperature or age of sediments (Schoell, 1988). Oxidants such as O_2, NO_3^-, Mn^{2+}, Fe^{2+}, and SO_4^{2-} are progressively depleted, based on energy yield, due to microbial activity within a sediment profile (Archer, 2007). Following the depletion of the other oxidants, methanogens reduce CO_2 using H_2, which results in a low energy yield (Thauer, 1998). Alternatively, methanogens may utilize simple organic compounds, such as acetate or formate, as their energy source (Madigan et al., 2003).

Methanotrophy is the dominant process through which soils act as a methane sink and it proceeds under either oxic or anoxic conditions. Methane oxidizing bacteria (MOB) are generally present in terrestrial systems and rely upon oxygen to oxidize methane (Aronson et al., 2013), whereas anaerobic oxidation of methane (AOM) is generally found in marine systems and relies on other oxidants, such as sulfate, to oxidize methane (Knittel and Boetius, 2009). AOM is estimated to consume around 90% of all biogenic methane within marine environments limiting the oceanic methane source strength to less than 2% globally (Hoehler et al., 1994; Knittel and Boetius, 2009). AOM is still, after over 30 years of investigation, an enigmatic process. It is however, generally agreed upon that AOM is the result of a methanogen-sulfate reducing consortium functioning at the SMTZ (Hoehler et al., 1994; Reeburgh, 2007; Knittel and Boetius, 2009).

The biogeochemical cycling of methane has been documented in other cold ecosystems including deep marine systems (Colwell et al., 2008), Arctic thermokarst

lakes (Walter et al., 2006), and permafrost (Wagner et al., 2005). In subglacial environments, organic substrates may be present from the sequestration of carbon during glacial overriding of vegetation or input from supraglacial throughflow (Sharp et al., 1999). At RG, organic carbon is around 1-3% dry sediment weight as determined from particulate organic carbon analysis of subglacial sediments (this research and Boyd et al., 2010) which is higher than in other subglacial systems (values are OC as a percentage of sediment dry weight: Lower Wright Glacier, Antarctica, 0.07 ± 0.03; Russell Glacier, Greenland, 0.44 ± 0.09; John Evans Glacier, Canadian Arctic, 0.20 ± 0.13; Engabreen, Norway, 0.19 ± 0.08 (Stibal et al., 2012)).

1.2.3 Glacial Systems

Glacial Distribution Past and Present Over Earth's 4.5 billion year history, 6 major glacial periods have been recognized. During the earliest, Precambrian glacial events, ice sheets may have covered low elevations at equatorial and mid latitudes such as proposed in the Neoproterozoic (Kirschivink, 1992). During the past 34 million years, Antarctic ice sheets have oscillated between glacial-interglacial periods, which are characterized by changing degrees of glacial coverage (Benn and Evans, 2010). Northern hemisphere glaciation began around 3.2 Ma (Benn and Evans, 2010). Northern ice sheets advanced to their most recent maximum extent, covering vast expanses of northern North America (Dyke et al., 2002), around 20,000 years ago, known as the Last Glacial Maximum (LGM).

Subglacial Sediments Subglacial sediments are generated through abrasion and crushing at the base of a glacier as it slides over its substrate. Because cold based or polar glaciers are frozen to their beds, little to no glacial erosion occurs at the base. Consequently, the majority of glacial biogeochemical activity occurs at polythermal or temperate glaciers where there is greater subglacial erosional activity than at cold based glaciers (Anderson, 2007). Sediment yields are up to 10 times greater in glaciated (warm-based) mountain catchments than in non-glaciated mountain catchments (Anderson, 2007). Through subglacial grinding and crushing, glaciers produce sediments with high mineral surface area per unit mass providing a weatherable surface. Chemical and microbially mediated weathering reactions with fresh sediment surfaces (Foght et al., 2004; Skidmore et al., 2005; Montross et al., 2013) contribute to solute fluxes from glacial catchments (Sharp et al., 2002; Anderson, 2007).

Subglacial sediments are exposed to atmospheric conditions at the terminus of a glacier during the ablation season due to glacial retreat. The rate of glacial retreat will determine the extent of subglacial sediment exposure over time. Once the subglacial sediments are exposed from beneath the glacial ice they are considered proglacial sediments as depicted in Figure 1.2. Direct access to subglacial sediments at RG via ice coring in the terminus region presented challenges due to the debris entrained within the ice. Attempts to access the subglacial sediments by drilling through the ice were unsuccessful. Therefore, the sediments sampled in this research are in the proglacial zone but represent those recently exposed from glacial retreat and are a reasonable proxy for subglacial sediments. We are confident that these sediments are recently exposed as

researchers have been at RG for 3 consecutive years (2011-2013) and have observed the retreating glacier terminus. The term glacial sediments will be used throughout this document in reference to the sediments sampled.

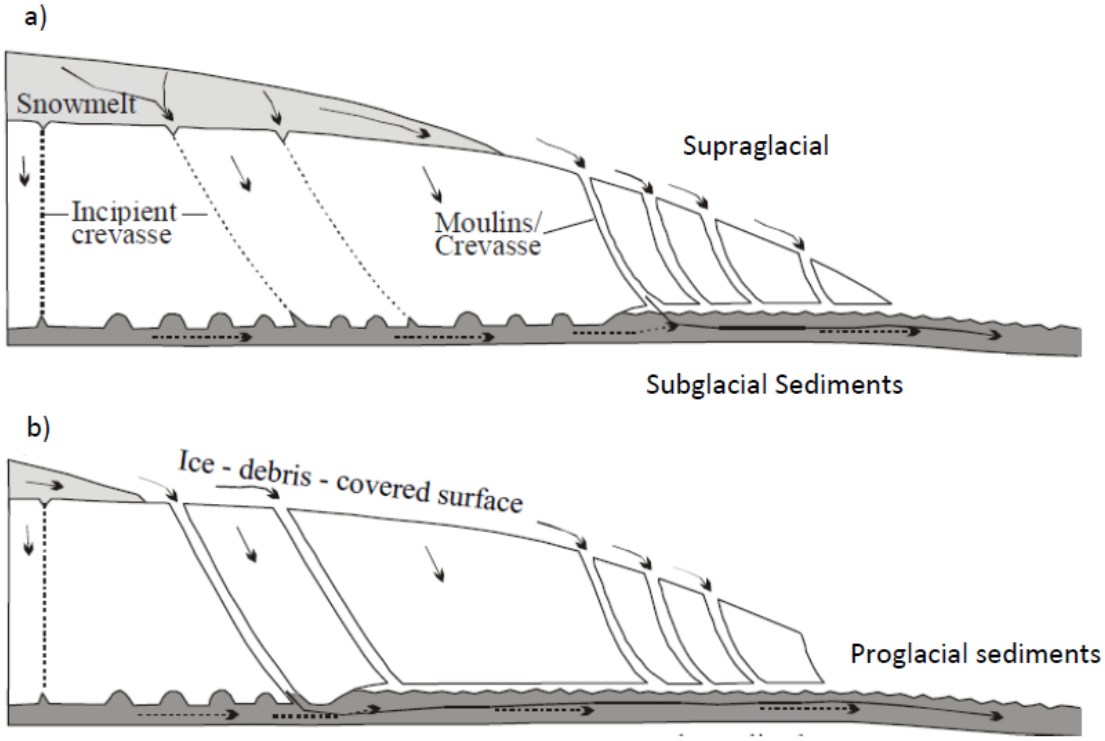

Figure 1.2: Images *a* and *b* depict a retreating glacier at two time points: T_0 (image *a*) and T_1 (image *b*). Subglacial sediments are exposed at the retreating front of the glacier and are then considered proglacial sediments. Arrows depict the direction of supraglacial (solid arrows) and subglacial (dashed arrows) water flow. Glacial retreat has been observed during the period 2011-2013 at Robertson Glacier, and was also observed over the 2012 melt season, July to September. Figure adapted from Montross (2007).

Subglacial Hydrology Glacial thermal regimes may be categorized as temperate, polythermal, or cold based on the extent to which they are frozen to the beds. This thermal regime along with other physical characteristics of the glacier will dictate the subglacial hydrological system which is formed from supraglacial, englacial and

subglacial contributions. The supraglacial waters contribute atmospheric gases (i.e. CO_2 and O_2) to the subglacial environment. Surface (supraglacial) meltwater may be routed to the glacier base via moulins and englacial cavities. Subglacial environments may be anoxic especially where distributed drainage systems are dominant and/or high organic matter content exists (Tranter et al., 2005), however, supraglacial waters may oxygenate the sediments and waters beneath the glacier (Figure 1.2). The supply of CO_2 and O_2 from supraglacial waters will affect both chemical weathering of sediments and microbial activity beneath a temperate glacier, like RG (Tranter et al., 2002; Benn and Evans, 2010; Montross et al., 2013).

Subglacial Ecosystems The presence of viable microbes in a range of subglacial environments is now supported by a significant body of evidence (Sharp et al., 1999; Skidmore et al., 2000; Campen et al., 2003; Foght et al., 2004; Skidmore et al., 2005; Wadham et al., 2008; Lanoil et al., 2009; Barcena et al., 2010; Boyd et al., 2010; Boyd et al., 2011; Nauer et al., 2012; Wadham et al., 2012; Hamilton et al., 2013). Microbial populations from supraglacial, subglacial and proglacial environments have been identified. Cell counts from these environments have been shown to correlate with sediment content in basal ice (Sharp et al., 1999) suggesting the importance of sediment substrate for microbial activity (Sharp et al., 1999; Skidmore et al., 2000; Foght et al., 2004). The subglacial sediments may provide both energy and nutrient sources that microbes require (Tranter et al., 2005). Geochemical and microbial evidence from RNA-based approaches indicates the presence of active methanogens in the subglacial sediments at RG (Boyd et al., 2010; Hamilton et al., 2013).

1.2.4 Broader Implications

During the last interglacial period there was a similar boreal forest extent as today and this environment would have been overridden during the LGM, burying the organic matter beneath glaciers and ice sheets (Skidmore et al., 2000 and references therein). The sequestered carbon from boreal forest, soils and other carbon rich ecosystems may have provided the carbon source for microbial activity beneath the warm based areas of Northern hemisphere ice sheets (Wadham et al., 2008). Where anoxic conditions existed, methanogenesis may have occurred (Tranter et al., 2005), resulting in a potential subglacial reservoir of methane (Wadham et al., 2008). Additionally, where ice sheet thickness exceeded several hundred meters, methane hydrates may have formed subglacially (Weitemeyer and Buffett, 2006). During the retreat of the ice sheets, the release of these gas reservoirs to the atmosphere may have had global climatic consequences. The rate at which the methane was released would determine the significance of its impact on atmospheric processes, such that a steady-state release over the period of retreat would be relatively small and insignificant (Brook et al., 2000; Stibal et al., 2012) but, more rapid methane release rates could result in increased atmospheric concentrations. Current modeling studies postulate large reservoirs of carbon-based gases beneath ice sheets (e.g. Antarctica (Wadham et al., 2012)) however; these one dimensional models use methane production rates based on experimental data (Wadham et al., 2012). This research presents the direct measurement of carbon-based gas release from glacial sediments.

1.3 Research Objectives

The primary objective of this research is to quantify the flux of methane from the glacial sediments at Robertson Glacier and improve our understanding of the driving forces behind the measured flux.

Objective 1: Quantify the average methane flux from glacial sediments to the atmosphere over a melt season and a) evaluate correlations of methane flux to sediment temperature, and fluxes of methanogenic substrates carbon dioxide and carbon monoxide, b) evaluate correlation of methane flux with time since exposure of the subglacial sediments due to glacial retreat and c) examine the spatial distribution of the methane flux parallel and perpendicular to the glacier terminus.

Objective 2: Analyze sediment cores to a) quantify concentrations of methane, carbon dioxide, carbon monoxide and hydrogen gas at a range of depths ($\leq$ 30 cm) within the sediment vertical profile, b) characterize sediment properties of porosity, porewater volume and particulate organic carbon, c) assess statistically significant relationships between the methane concentrations, other gas analytes and sediment properties at depth within the vertical core profiles and d) calculate a diffusive flux of methane for comparison to the net surface methane fluxes measured via the static chamber method.

CHAPTER 2 - METHODS

2.1 Study Site

Robertson Glacier (RG) is located at 115° 20' W, 50° 44' N, in Peter Lougheed Provincial Park near the provincial boundary of British Columbia and Alberta, Canada. RG occupies a north-south trending valley and is approximately 3 km long, ranging in altitude from 2370-2900 m. RG has been the site of prior research including bedrock geology mapping (McMechan, 1998), analysis of runoff composition and mineral weathering (Sharp et al., 2002; Mitchell et al., 2013) and microbial community investigations (Boyd et al., 2010; Boyd et al., 2011; Hamilton et al., 2013). The catchment bedrock is of a calcareous composition, largely limestone and dolomite, with interbeds of shale, siltstone and sandstone (McMechan, 1998). Basal sediments and bedrock are exposed at the terminus of the glacier as it is currently retreating (Figure 2.1). There is limited insolation at RG due to steep headwalls bounding the east and west sides of the glacier. The proglacial sediment temperatures remain low, at an average of 6.1^{o}C at 5-10 cm depth next to each GFC from July 16th to September 22nd, 2012. There are two subglacial melt water streams draining the glacier, Robertson east (RE) and Robertson west (RW), with RW being the dominant stream with a well-defined and partially incised channel at the terminus. There is an ephemerally saturated zone at the glacier terminus where several small melt streams drain and then coalesce in the glacier forefield to form the RE stream which flows in a defined channel ~ 40 m downstream from the RG terminus. During the 2011 and 2012 melt seasons there was retreat of the

ice margin upslope due to ablation exposing subglacial sediments. These recently exposed subglacial, now proglacial *(sensu strictu)* sediments, are the focus of the study as they are the closest easily accessible proxy for subglacial sediments.

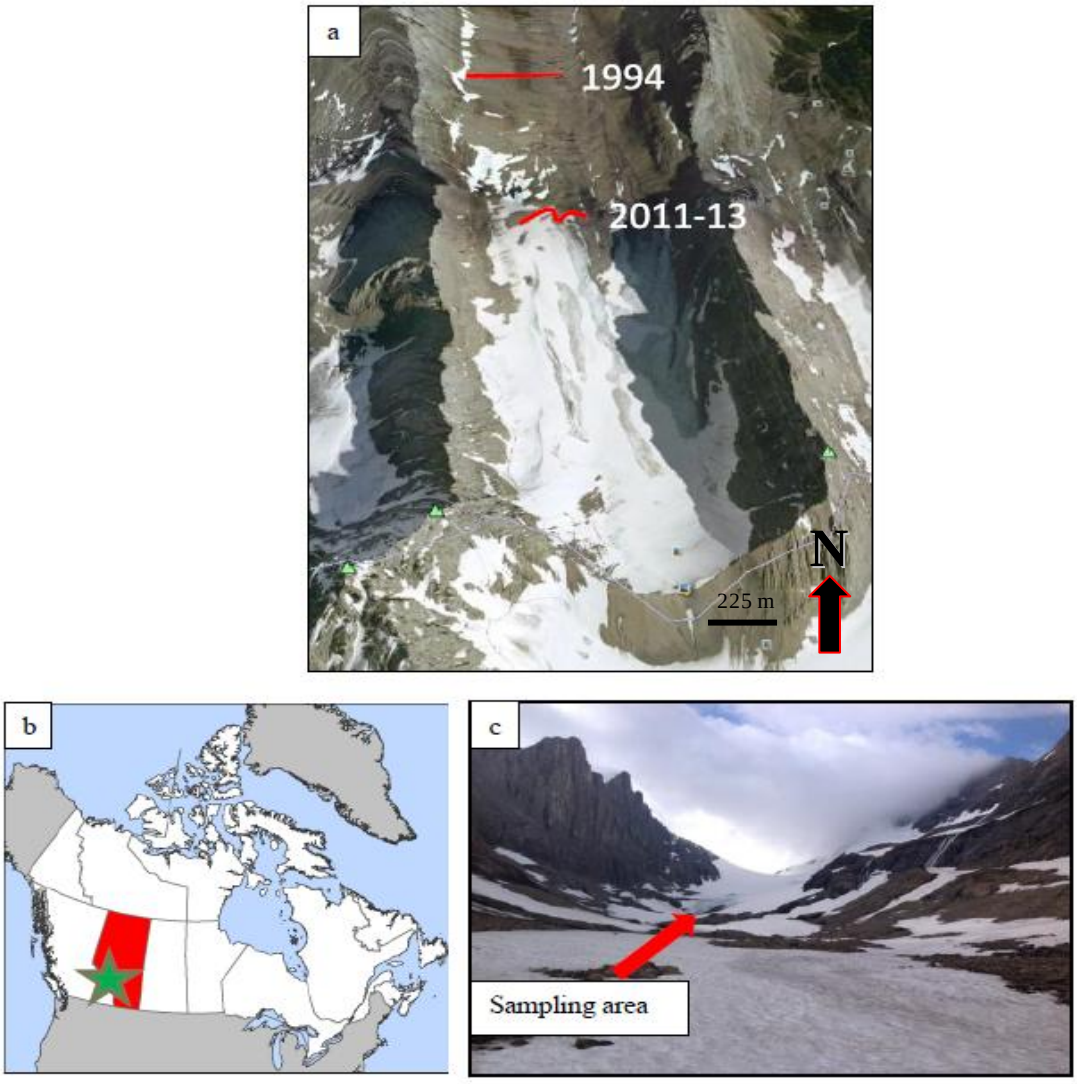

Figure 2.1. Image *a*: Satellite image of Robertson Glacier (RG) from Google Earth. Approximate glacier terminus positions for 1994 and 2011-2013 are shown. GPS data courtesy of M. Skidmore and J. Dore. Note the steep headwalls on either side of the glacier limiting insolation year round. Image *b*: Location map for RG. Image *c*: (July 20th, 2012) Looking south, up glacier, annual snow fields are in the foreground and the proglacial sampling area is within 50 m of the glacier terminus during field season 2012.

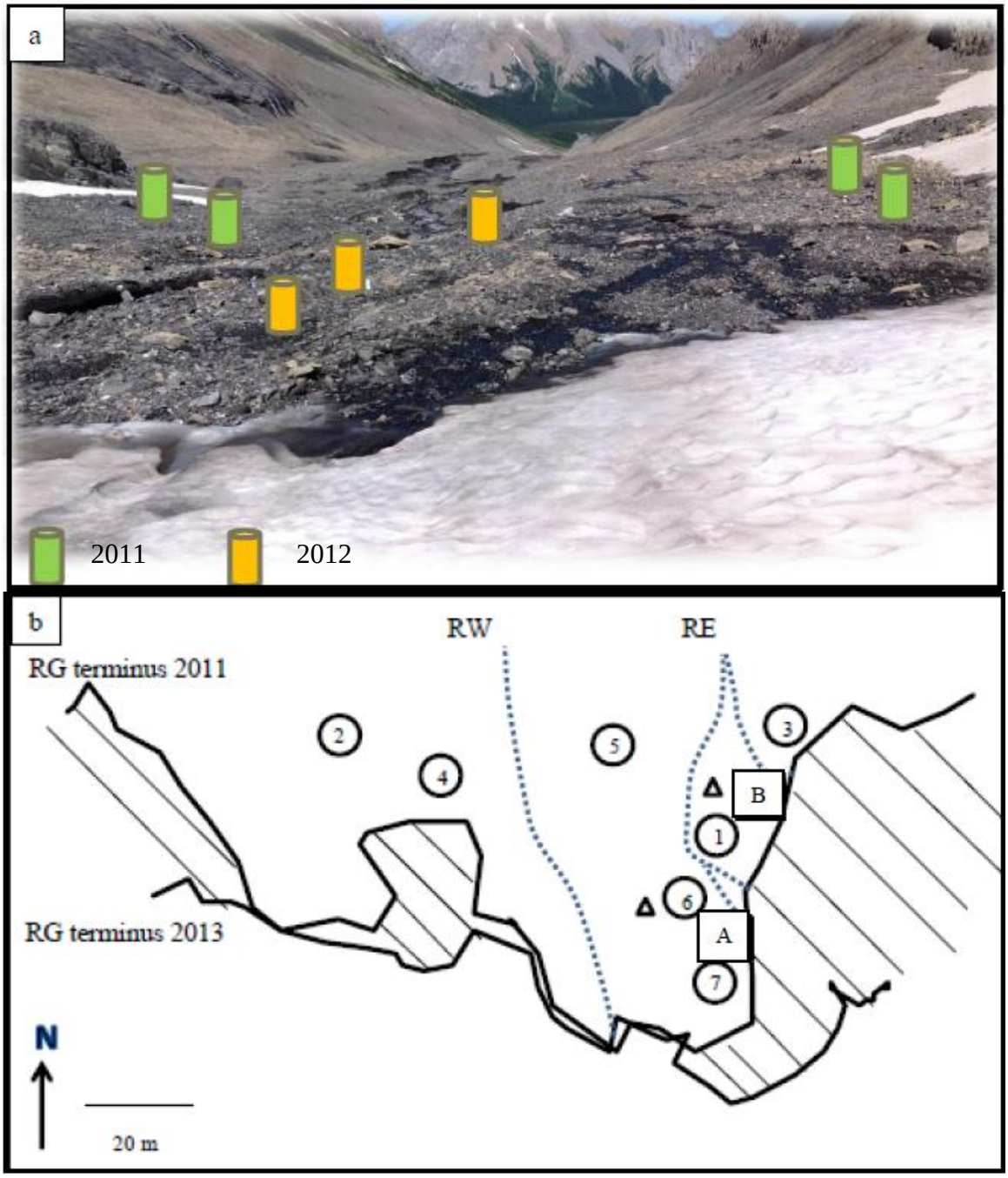

Figure 2.2. Upper image (a) shows the relative locations for the surface gas flux chambers in the proglacial area. Lower image (b) is a diagram of the proglacial sampling area. Triangles are locations of temperature loggers at 5 cm depth during melt season 2012. Squares, A and B, denote the locations of the depth trio GFCs. Dotted lines are the locations of the glacial melt drainages RW (Robertson west) and RE (Robertson east). Hash marks show the retreat of RG terminus 2011 to August 2013. All GFC and glacier terminus points based on GPS coordinates collected August 2011 and August 2013 via Garmin GPS map 76S courtesy of J. Dore.

2.2 Static Gas Flux Chambers

Gas flux chambers (GFCs) were deployed in the proglacial area of RG to measure the gas fluxes of methane from the recently exposed subglacial sediments (see Figure 2.2 for locations). Four GFCs were deployed during field season 2011 and an additional 6 chambers during field season 2012. Two different GFC designs were employed and referred to hereafter as surface chambers and depth chambers (Figure 2.3 and Figure 2.2b). Of the 10 GFCs deployed, 7 were surface and 3 were depth chambers.

2.2.1 GFC Design and Deployment

Surface GFCs were constructed of 10 cm diameter open-bottomed, white PVC tubes, 30.5 cm in length, and capped at one end with a rounded PVC cap fitted with two ports. A length of Teflon tubing, approximately 50 cm per port was fitted to each port hose adapter (Figure 2.3). To minimize gas loss from the chamber headspace the tubing ends were fitted with quick release male and female connectors to enable rapid connection to a Vaisala GM70 hand-held CO_2 meter, equipped with a small battery operated pump. This allowed circulation of the headspace gases through the meter. The connection for the CO_2 meter also contained a sampling port with a septa fitting for extraction of discrete gas samples for analysis via gas chromatography. Measuring a gas flux in this particular environment required some amendments to a standard gas flux chamber sampling methodology as described by Parkin and Venterea (2010). In this study a 3-day sampling period with 24 hour sampling intervals was determined empirically to be the optimum sampling frequency due to slow accumulation of gas in the GFC headspace. The surface GFCs were placed into the sediments at an average depth of

5 cm and rocks were placed around the chambers to act as an anchor. The volume to surface area ratios (54.1-27.2) for the GFCs were higher than recommended (i.e. >10) in the GRACEnet protocols (Parkin and Venterea, 2010) and a larger than recommended sample was extracted (50 ml as opposed to the recommended 30 ml). However, the gas sample volume (50 ml) was still within GRACEnet protocol recommendation as it was proportionally less of the overall volume due to the large chamber volume. A larger surface area chamber would be difficult to anchor into the variable, rocky terrain and would pose increased risk of leakage. Six to eight 4 cm length slats were hacksawed into the open bottom of the PVC cylinder to minimize chamber obstruction of fluid flow through the sediments. The GFCs were left in place for the duration of the sampling season. Relative humidity (RH) and temperature were measured in the chamber simultaneously with CO_2 via the Vaisala meter and were within 2% of atmospheric conditions indicating little perturbation by the chamber on these variables. It was expected that gas accumulation in the flux chambers would be slow and that values would be relatively low based on the 2011 trial season. Therefore, to prevent loss of gas from the headspace no vent tubes, used for pressure perturbations, were installed.

A sampling transect perpendicular to the glacier terminus was established with GFCs 5-7 while GFCs 1-4 were placed within 20 m of the glacier terminus as a parallel transect (Figure 2.2). The GFCs of the perpendicular transect were 20-30 m apart. GFCs 1 and 5-7 were located on a sediment terrace bounded to the west by RW drainage which exposes a bank of the terrace to a depth around 3 m. The eastern boundary of the terrace is a small ephemeral stream which has exposed the terrace to around 1 m depth. The

multiple small streams forming RE drainage drain the terrace near to the glacier terminus before descending over the terrace edge to eventually join RW downstream of the sampling area. GFCs 1, 6 and 7 are located near the multi-stream area of RE and GFC 5 is furthest north along the terrace around 50 m from the glacier terminus. GFCs 2-4 are located off the sediment terrace in shallower sediment deposits. Sediment depth proximal to GFCs 2, 3, and 4 was determined through core sampling where cores no greater than 15 cm were recovered before reaching the underlying bedrock. GFC 3, the eastern most GFC, is near the small ephemeral stream that bounds the terrace to the east. GFCs 2 and 4, the western most GFCs, are near bedrock outcrops and also located in shallow sediment deposits.

Depth GFCs, three smaller volume gas flux chambers, referred to also as the depth trio, differed from surface GFCs in several ways. Depth chambers were 50 cm in length, with a diameter of 6.35 cm and the opening at the base was covered with Gortex™, held in place by a hose clamp to prevent water from entering the chamber. The depth trio was designed to be a mobile set to compare, at a given location, gas fluxes at 5, 10 and 15 cm depths. These chambers were placed 20 cm from each other in holes dug to the specified depth with overlying sediments removed. The trio was placed in two different locations in the proglacial area during the 2012 melt season (see Figure 2.2). Location *a*, July 28th to August 27th was slightly northeast of GFC 1 on a small mound of sediment which dried out during the field season due to melt stream movement away from the mound. Location *b*, Sept 1st to Sept 22nd, was south of GFC 7 and was closest to

the glacier terminus in an intermittently saturated zone that remained wet over the field season as the glacier retreated.

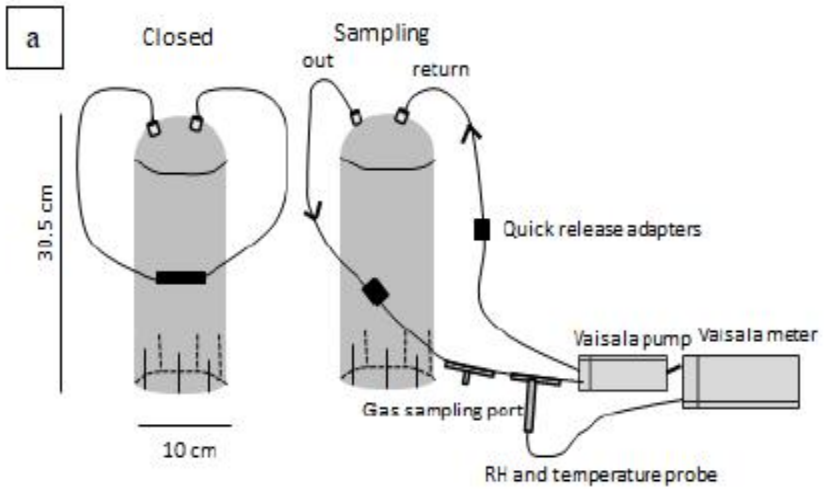

Figure 2.3. Image *a* is a schematic of gas flux chambers during closed and sampling modes. Depth chambers in image *b* are compared to the surface chamber in image *c*. Sampling methods were identical for surface and depth chambers. Note the "closed" set up for the GFC in image *c*. Image *c* also shows the Vaisala GM70 hand-held CO_2 meter (left), equipped with a small battery operated pump (center) in the plastic carrying case.

2.2.2 GFC Gas Sample Collection

A sampling period for a GFC (surface or depth) was comprised of 3 sampling points each approximately 24 hours apart. Four sampling periods were conducted during the 2011 field season from July to September. These 4 sampling periods were used to evaluate sampling methods and determine a strategy for the 2012 field season. Ten sampling periods were conducted during the 2012 field season spanning the period from July 28th to September 22nd and these data are presented in chapter three. GFC sampling ports were left open between sampling periods so the GFC headspace could equilibrate with atmospheric conditions. More than 80% of the time (82 out of 102) the initial headspace concentrations were within 10% RG atmospheric methane concentration (1.81 ppmv). During sampling, the Vaisala CO_2 meter was attached to the in and out port hoses on the GFC and headspace gases were circulated through the infrared sensor for CO_2 measurement using a small battery operated pump. CO_2, RH and temperature measurements inside the GFC were recorded for 10 minutes. A 50 ml sample of chamber headspace gas was removed via syringe through a septum-fitted sampling port integrated in the sampling hose, and then transferred into a 200 ml, 4-ply SKC™ FlexFoil Plus air tight gas sampling bag with a polypropylene hose/valve and septum fitting. The GFC port hoses were then connected to create a closed system after detachment from the Vaisala meter. A similar process was conducted on days 2 and 3 except the hoses were left unconnected on the final, third day of sampling to allow equilibration with the atmosphere prior to the next sampling period. Sampling period 9, September 13-14, was unique in that we sampled 3 times over 24 hours. Fluxes from this sampling period were calculated from 2 point rates (T_o-T_{24}).

2.2.3 Ambient Sample Collection

A 200 ml sample of atmospheric air at RG terminus was collected once per sampling period. Four 50 ml air samples were collected, ~ 1 m above the sediment surface, via a 50 ml syringe and injected into a labeled 200 ml SKC™ gas sampling bag. Ambient RH and temperature were measured with the Vaisala probe prior to sampling at each GFC. Efforts were made to record temperature and RH in shaded areas at all GFCs. Sediment temperatures were recorded at each GFC approximately 10 cm below the surface with a soil temperature probe. A thermistor and Hobo™ data logger recorded continuous sediment temperatures at two locations; one near GFC 2 and one near GFC 7, in the proglacial area at a depth of 5 cm for the duration of the field season (see Figure 2.2).

2.2.4 Gas Analyte Measurements

A gas chromatograph (GC) was used to measure the gases of interest in the headspace samples collected from the GFCs. An SRI 8610C GC was equipped with a flame ionization detector (FID) for the simultaneous analysis of carbon monoxide (CO), carbon dioxide (CO_2), and methane (CH_4). Helium was used as the carrier gas at a pressure of 22 psi. The methanizer was set to 330^{o}C and the column oven temperature to 40^{o}C. The FID was plumbed with either a Restek Shin Carbon ST 80/100 (2 m) column or a Restek Porapak Q SS (1.8 m) column depending on analytes to be sampled. The Porapak Q column was used for 4 minute isothermal GC runs, backflush at 0.4 minutes, for CH_4 analysis and were conducted within 24 hours of sample collection. The Shin Carbon column was used to measure all gases (CO, CO_2, and CH_4) in a temperature ramp

17 minute run (ramping from 40°C to 90°C over 10 minutes, hold for 5.5 minutes, ramping up to 161.5°C over 13 minutes and then back down 40°C holding for 1 minute) with a backflush at 0.7 minutes and were conducted within 7 days of sample collection. A 3 ml sample was extracted via needle and syringe from the SKC™ airtight gas bag and injected through a septum in the GC sampling valve port onto the 1 ml sample loop. The peak areas were integrated using Peak Simple™ software.

2.2.5 Gas Standards

Gas standards were prepared and run before, during and after sampling to build a calibration curve. A certified gas standard was purchased from American Gas Group (Toledo, Ohio) of 1% CO, CO_2, CH_4, H_2, O_2 with the balance N_2. Working standards spanning 1 to 1000 ppm were made using serial dilution and ultra-high purity (UHP) N_2 as the matrix gas. New batches of working standards were made weekly during regular gas sampling.

2.2.6 GFC Gas Flux Calculations

The peak areas integrated from the Peak Simple™ software were converted to moles of gas using the standard calibration curve. The mole fraction of the analyte, *x'*, in ppmv, was then calculated based on the ideal gas law.

$$x' = 10^6 RT \left(\frac{n}{V}\right) / P \qquad \text{(Eq 2.1)}$$

Where

R = ideal gas constant (0.082 L atm mol^{-1} K^{-1})

T = sample loop temperature (K)

n = moles of gas

V = sample loop volume (L)

P = laboratory air pressure (atm)

The analyte concentrations (ppmv) at each sampling point; T_0, T_1, and T_2 corresponding to times 0, 24 and 48 hours, were used to calculate a rate of change in gas concentration over time (Figure 2.4). The quadratic regression (QR) model as described by Wagner et al. (1997) was used to calculate the rate. This model assumes that the gas flux chamber will have an effect on the flux of gas from the sediment to the atmosphere referred to as the "observer effect". To determine the flux in the absence of the chamber, the first derivative of the quadratic equation is used because it describes the instantaneous rate of change. The rate of change is the slope of the line tangent to the curve as it crosses the y-axis (at time 0); the tangent line is the best linear approximation of the parabola at that point. If only two data points were used the quadratic regression was the same as a linear regression model.

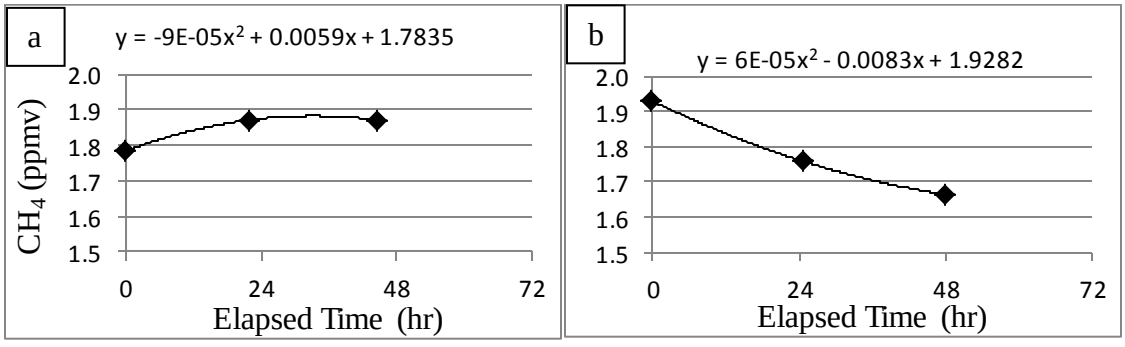

Figure 2.4. Methane concentration changes over time as measured in the GFC headspace. Graph *a* shows a positive rate and graph *b* shows a negative rate. Graph *a* data is from GFC 2 July 28th -30th, 2012 and graph *b* data is from GFC 3 August 2nd - 4th, 2012. A second order polynomial curve was applied to the data. The slope of the curve as it crosses the y-axis is the instantaneous rate of change used to calculate the flux.

The observer effect was added as a second order term to the linear equation

$$f\ x\ = ax^2 + bx + c \qquad \text{(Eq 2.2)}$$

Where *a* is the speed of increase (or decrease), *b* is the declivity of the parabola and *c* is the y-intercept. The first derivative of equation 2.2:

$$f'\ x\ = 2ax + b \qquad \text{(Eq 2.3)}$$

where setting the time (*x*) to zero gives the rate (*b*) as it is assumed to be in the absence of the observer effect.

$$f'\ x\ = b \qquad \text{(Eq 2.4)}$$

From the rate, a flux (*J*) was calculated taking into consideration the ground surface area covered by the GFC, volume of the GFC, temperature, pressure and the moisture mixing ratio within the GFC following LI-COR (2012).

$$J = \frac{10^4\ V P\ 1 - \frac{W_0}{1000}\ \frac{\partial C}{\partial t}}{RST} \qquad \text{(Eq 2.5)}$$

Where: R = ideal gas constant (8314.5 cm^3 kPa mol^{-1} K^{-1})

T = temperature (K)

V = volume (cm^3)

P = pressure (kPa)

W_0 = initial water vapor mole fraction (mmol mol^{-1})

S = surface area (cm^2)

$\frac{\partial C}{\partial t}$ = rate of change in headspace gas concentration over time (ppmv sec^{-1})

The same algorithm was applied to calculate both CO and CO_2 fluxes. However, CO_2 flux calculations used data from the Vaisala GFC headspace concentration measurements instead of GC measurements. Fluxes were calculated and reported only for rates where the initial headspace concentration was within a percentage of RG atmospheric concentrations: CH_4 T_0 within 10% RG atmospheric concentration (averaged over the melt season), CO_2 T_0 within 6% of RG atmospheric (measured at T_0 for each sampling period) and CO T_0 within 200% of RG atmospheric concentrations (averaged monthly except for sampling period 10 which used contemporary atmospheric data). CO initial headspace concentrations were much higher than atmospheric at the time of sampling. This may indicate either exceptionally high CO fluxes from the sediments or an analytical error, however, no analytical errors were found. Interpretation of the CO flux data should be considered with caution in light of these unusually high atmospheric CO concentrations.

2.3 Vertical Sediment Cores

Sediment cores were collected within 50 m of the terminus of Robertson Glacier (RG) based on the protocol of Boyd et al. (2010). All cores were collected in proximity to gas flux chambers for comparison with nearby gas flux data (see Figure 2.5 for all sampling locations). Cores were collected to 1) quantify concentrations of methane, carbon dioxide, carbon monoxide and hydrogen gas at a range of depths (≤ 30 cm) within the sediment vertical profile, 2) characterize sediment properties of porosity, porewater volume and particulate organic carbon, 3) assess statistically significant relationships between the methane concentrations, other gas analytes and sediment properties at depth

within the vertical core profiles and 4) calculate a diffusive flux of methane for comparison to the net surface methane fluxes measured via the static chamber method.

2.3.1 Sediment Core Collection and Sample Preparation

Sediment cores were collected in 6.4 cm diameter stainless steel casings ranging from 15-30.5 cm in length. The steel casings were pounded vertically into the sediments using a mallet and pounding cap. To ensure no loss of sediment a shovel was used to aid in the extraction of the core by digging a small trench towards the bottom of the casing and prying the core out of place. PVC caps, rounded in 2011 and flat in 2012, were placed on both ends of the core casing after removal of all sediment and debris from the outside of the casing to ensure a clean, tight seal. Cores were labeled and immediately placed in an insulated storage container with ice packs for transport out of the field and then placed in a -30^{o}C freezer within 4 hours of collection.

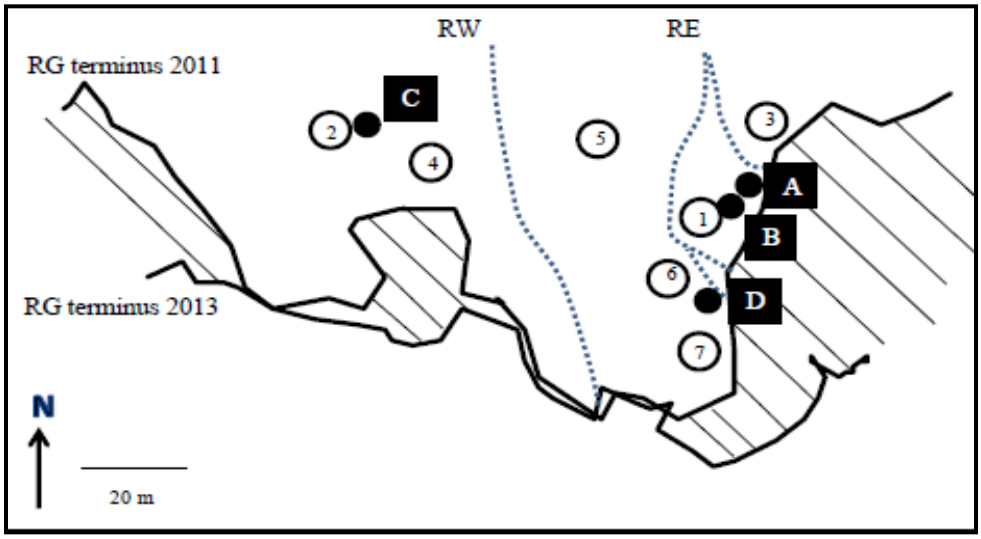

Figure 2.5. Robertson Glacier terminus and proglacial core collection sites. Solid circles denote core location relative to nearest GFC (1-7) and the cores are labeled A-D. Cores A and B were collected on July 11, 2011 and cores C and D on August 8 and September 8, 2012, respectively.

The frozen cores were cut at -20°C in the Subzero Science and Engineering Research Facility at Montana State University. In brief, cores were placed in a jig and two longitudinal cuts were made through the steel casing with a circular saw to remove the casing from the sediment core. Cores were subsampled in 3-5 cm increments, referred to as pucks, for subsequent analysis. Pucks were cut using an angle grinder fitted with a diamond blade.

The 2011 core pucks were halved, one half for sediment and gas analysis and the other for future microbial analysis. For the 2012 core samples, the pucks were further divided approximately in quarters for analysis; three of the quarters for triplicate gas and sediment analysis and the other quarter for future microbial analysis. Microbial subsamples were placed in a labeled whirlpak and stored in a -80°C freezer. Each subsample allocated for gas and sediment analysis was placed in a preweighed, sterile 125 or 250 ml I-chem® septa cap jar along with a 2" x 5/16" stir bar. The headspace of the sample containing I-chem® jar was purged with ultra-high purity nitrogen gas (UHP N_2) for 2 minutes during which time all atmospheric gas in the headspace was displaced by the UHP N_2. Sample jars were then reweighed and stored upside down (to prevent any gas loss) in a -30°C freezer prior to gas sampling. Controls were prepared in tandem with samples and all analytical procedures were conducted on controls except for the addition of sediment.

2.3.2 Sediment Gas Sampling

Sediment puck subsamples were removed from the -30°C freezer and thawed overnight at 4°C. A sediment slurry was made prior to gas sampling by injecting 20 ml

of degassed, 18.2 MΩ ultrapure H_2O into the sample jar. Prior to injection the 18.2 MΩ ultrapure H_2O was degassed using a combination of sparge and vacuum techniques. The water was sparged with UHP N_2 for 5 minutes, and then attached to a vacuum to remove the headspace gas. This process was repeated three times to achieve levels of methane, carbon dioxide, carbon monoxide and hydrogen gas in the water at or below the detection limit of 1 ppmv of the SRI8610C gas chromatograph (GC). The sediment slurry was allowed to equilibrate while agitated on a stir plate for 15 minutes at 22°C (room temperature). A 10 ml sample of the headspace was extracted through the septa and injected through a hose on the injection valve port of the GC.

2.3.3 Gas Chromatography

In addition to the FID used for GFC gas headspace analysis, a pulsed discharge helium ionization detector (PDHID) was used for the simultaneous analysis of carbon monoxide, carbon dioxide, methane and hydrogen gas (CO, CO_2, CH_4, and H_2, respectively). Helium was used as both the carrier and discharge gas for the PDHID at flow rates of 20 ml/min (carrier gas) and 4 ml/min (discharge gas). H_2 was measured with the PDHID plumbed with a 2 ml loop in sequence with Hayesep D (1.8 m), Hayesep DB 100/120 (4.5m), and molsieve 13x (1.8 m) columns (see schematic in Appendix A).

2.3.4 Glass, Metal and Plasticware Preparation

All utensils and labware were cleaned and sterilized prior to use. Glassware was washed with soap and water, rinsed 3x with deionized (DI) water, soaked in a 1 M HNO_3 bath for 1 hour, re-rinsed with DI water (3x), rinsed 3x with 18.2 MΩ ultrapure water and finally foil capped and furnaced for 4 hours at 550°C. Plastics were cleaned and

sterilized similarly except for furnacing which was replaced by foil wrapping the plastics and autoclaving at 123°C for 20 minutes. Metal utensils were also autoclaved but not placed in the 1 M HNO_3 bath.

2.3.5 Sediment Characterization

Water Content Sediment water content was determined via gravimetric methods. The remaining slurry in the 50 ml Falcon tube was reweighed and placed in a class 1000 laminar flow hood to air dry overnight at room temperature. The sediments in their respective containers were reweighed to determine water content lost. Sediments were further dried overnight in a 105°C oven and reweighed to determine residual water content.

Particulate Organic Carbon (POC) Organic carbon content in the sediments was measured gravimetrically. Sediments dried at 105°C (DW_{105}) were weighed and placed in a 550°C oven and baked for 5 hours to combust all organic carbon (Heiri et al., 2001). The sediments (DW_{550}) were reweighed after combustion to determine organic carbon content. The loss on ignition at 550°C (LOI_{550}) is the particulate organic carbon content as a percentage of the dry sediment weight.

$$LOI_{550} = ((DW_{105} - DW_{550})/DW_{105}) * 100 \quad \text{(Eq 2.6)}$$

Sediment Volume The bulk volume of each subsample was determined through gravimetric methods. The dried sediment volume was calculated from an assumed density of 2.4 g cm^{-3} (based on the average density of Devonian aged limestone and unconsolidated glacial material (Manger, 1963)) and the measured dry mass. The

measured porewater volume (based on assumption that density of water = 1.0 g cm^{-3}) was summed with the dried sediment volume to calculate the bulk volume of the subsample.

$$\frac{(m_{sedS})}{2.4} + V_{pw} = V_{bulk} \qquad \text{(Eq 2.7)}$$

If the sample was not at 100% saturation the calculated bulk volume would underestimate the true bulk volume. So, the bulk volume is considered a minimum volume for each sample.

2.3.6 Gas Concentration Calculations

Total concentration of gas, (C_t), per unit volume of bulk sediment (V_b) including void volume, was calculated from the sum total moles of gas in the headspace (n_h) and solution (n_s) for each subsample, minus moles of gas in negative control headspace (n_{ho}) and negative control solution (n_{so}).

$$C_t = (n_s + n_h - n_{ho} - n_{so})/V_b \qquad \text{(Eq 2.8)}$$

All measured peak areas from the GC were converted to mole fractions (x') via standard curves. The partial pressure of the gas of interest (P_g) is based on Dalton's Law where the mole fraction of gas is equal to the partial pressure of gas as a proportion of the total pressure of gas (P_t).

$$x' = P_g/P_t \qquad \text{(Eq 2.9)}$$

From Henry's Law and Henry's coefficient, k, which is replaced with the Bunsen coefficient (β), k = 1/β, where applicable (see Table 2.1 for β values used for each gas) the concentration of gas in solution (C_s) was calculated.

$$P_g = C_s k \qquad \text{(Eq 2.10)}$$

And the concentration of gas in the headspace (C_h) was calculated.

$$C_h = \frac{P_g}{RT} \qquad \text{(Eq 2.11)}$$

Where the ideal gas constant, R = 0.082 L atm mol^{-1} K^{-1} and T is temperature in degrees Kelvin.

Table 2.1. Bunsen solubility coefficients (β) in units of ml of gas dissolved in 1 ml of H_2O at STP.

Analyte	β	Reference
CH_4	0.03396	Weisenberg and Guinasso, 1979
CO_2	0.85081	Weiss, 1974
H_2	0.01792	Weisenberg and Guinasso, 1979
CO	0.02313	Weisenberg and Guinasso, 1979

CHAPTER 3 – RESULTS

3.1 Static Gas Flux Chambers

Methane (CH_4) concentrations were measured from gas flux chamber headspace samples from mid-July to the end of September, 2012, to quantify the flux of methane from the recently exposed subglacial sediments. Of the 295 gas samples collected and analyzed, 7 were removed from the data set due to sample contamination (i.e.: holes in the gas bags, open valves, GFC perturbations) and 20 were removed because T_o concentrations were outside 10% of the RG atmospheric concentration. A total of 82 rates and corresponding sediment to air fluxes were calculated from the remaining 268 CH_4 concentrations, 54 of these fluxes were surface GFC fluxes and 28 depth GFC fluxes. Of the 82 rates, 18 were based on 2 data points and the other 64 were based on 3 data points[2].

A permutation test was run to determine if the GFC methane headspace concentrations collected at each sampling point were significantly different than ambient concentrations of methane. ANOVA statistical analysis was conducted to determine if sampling period average fluxes for all surface GFCs were equal to one another. ANOVA statistical analysis was also conducted on the spatial distribution of the methane fluxes to determine if a) all sampling locations demonstrated equal average fluxes of methane for the duration of the melt season and b) if the average methane fluxes in the perpendicular transect GFCs were equal for the duration of the melt season. Additionally, regression

[2] values do not equal 288 because one sample was a singular data point from which a flux cannot be calculated.

analysis was conducted to determine the strength of correlations between the flux of methane and the following: sediment temperature, flux of carbon monoxide (CO) and flux of carbon dioxide (CO_2).

3.1.1 Methane Concentration Statistical Analysis

The CH_4 concentrations measured from all the GFC headspace samples ranged from 1.44 to 4.01 ± 0.02 (standard error) ppmv. A permutation test was run at each time point to determine if the values were significantly greater than RG ambient methane concentrations. The average RG ambient methane concentration of 1.81 ppmv ± 0.11 (1σ) was determined from ambient gas samples collected on July 28th, August 2nd, 7th and September 1st, 7th, 13th and 20th. A one sample, one tailed (greater than) t-test in the statistical program R v2.15 was run to test the null hypothesis that the methane headspace concentrations at each time point, T_0, T_1 and T_2, (0, 24 and 48 hours, respectively) for all, surface and depth, GFCs were equal to RG ambient concentrations. The null hypothesis can be rejected for time points T_1 and T_2 for all GFCs, surface and depth, during all sampling periods (July through September) at a significance level of $\alpha = 0.05$ (see Table 3.1).

3.1.2 Trends in Gas Analyte Fluxes

A comparison of surface methane fluxes over the melt season reveals a high degree of variability both spatially and temporally (see Figures 3.1 and 3.5). The sediment to atmosphere surface methane fluxes ranged from -3.08 to 11.02 μmol m^{-2} d^{-1} with a mean of 0.22 ± 0.27 (standard error) μmol m^{-2} d^{-1} (n = 54). The strongest surface efflux was measured in GFC 1 located near the glacier terminus in the ephemerally

saturated area on the sediment terrace. The most negative surface flux was measured at GFC 6 along the perpendicular transect. The spatial distribution of positive and negative fluxes for the gas analytes (CH_4, CO_2 and CO) tend to be associated with the sediment water content along the sediment terrace transect (Figures 3.1-3.4). Positive fluxes cluster in proximity to the glacier terminus (Figure 3.4) which coincides with higher sediment water content (Figure 3.6).

Table 3.1. Mean value, μ, one standard deviation, 1σ, and one way greater than p-value from a one sample t-test using the program R. v2.15. Values are from all GFC headspace methane concentration measurements including replicate

Sampling point	μ and 1σ	One–way greater than p-value	n
T_0	1.79 ± 0.15	0.92	108
T_1	1.87 ± 0.32	0.04	106
T_2	1.89 ± 0.38	0.03	97

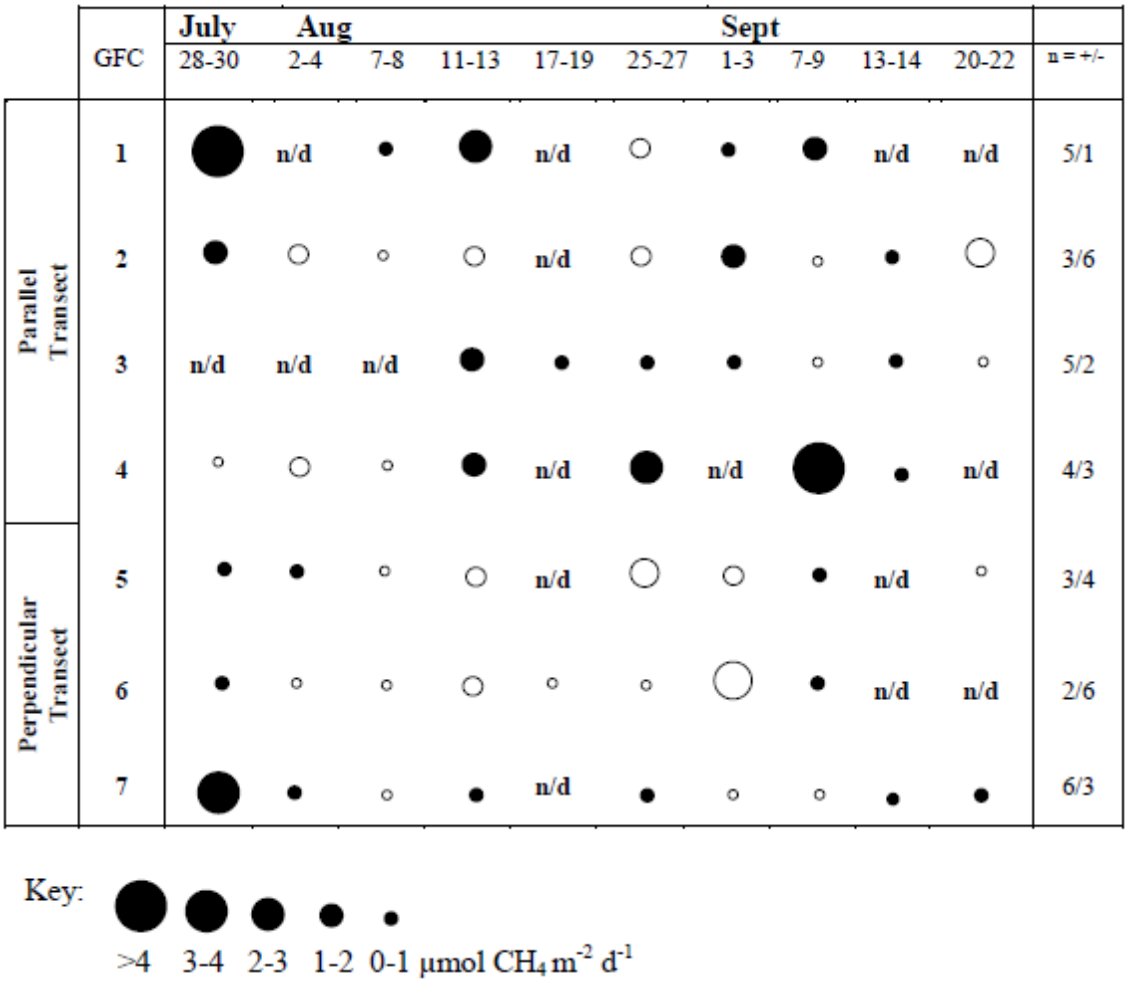

Figure 3.1. Matrix diagram showing CH_4 fluxes for surface GFCs for all sampling periods. Filled circles are positive fluxes and open circles are negative fluxes. The size of the symbol is proportional to the measured flux as shown in the key below the figure. The right hand column, n = +/-, is the total number of positive (+) fluxes vs negative (-) fluxes as a ratio measured during the 2012 melt season. GFC 7 is closest to the glacier in the perpendicular transect and n/d denotes times when no flux data is reported due to either the initial CH_4 headspace concentrations outside 10% of RG atmospheric concentrations or methodological problems (e.g. holes in gas bags, GFCs buried in snow).

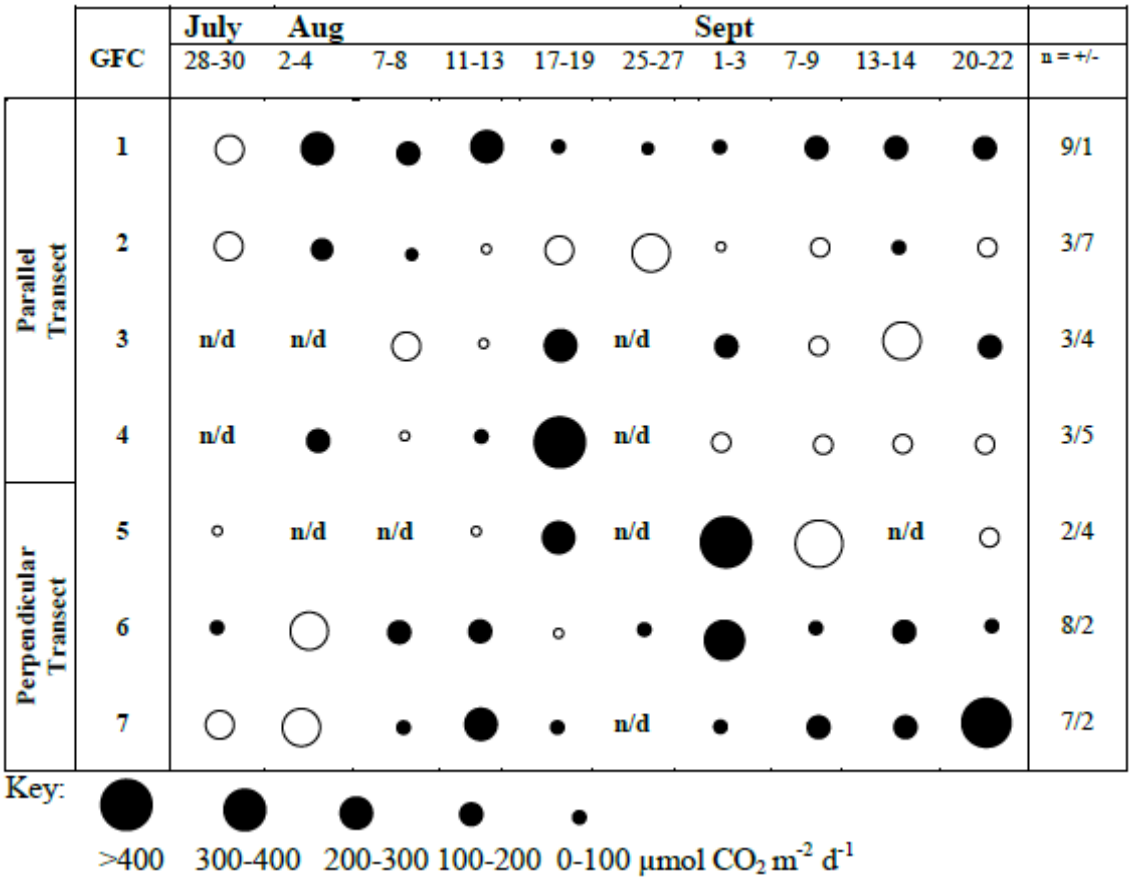

Figure 3.2. Matrix diagram showing all CO_2 fluxes for surface GFCs for all sampling periods. Filled circles are positive fluxes and open circles are negative fluxes. The size of the symbol is proportional to the measured flux as shown in the key below the figure. The last column, n = +/-, is the total number of positive (+) fluxes vs negative (-) fluxes as a ratio measured during the 2012 melt season. GFC 7 is closest to the glacier in the perpendicular transect and n/d denotes no flux data for that sampling period due to the initial CO_2 headspace concentration outside 6% of RG atmospheric concentrations.

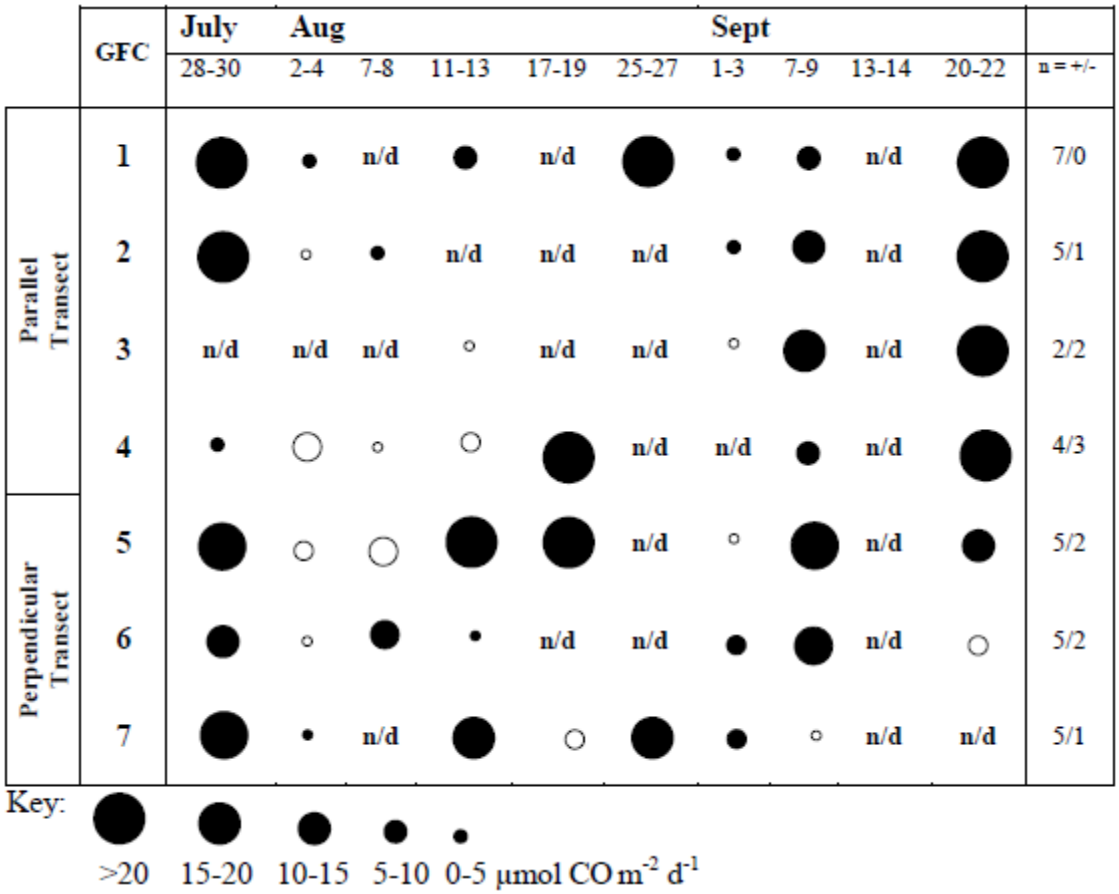

Figure 3.3. Matrix diagram showing all CO fluxes for surface GFCs for all sampling periods. Filled circles are positive fluxes and open circles are negative fluxes. The size of the symbol is proportional to the measured flux as shown in the key below the figure. The last column, n = +/-, is the total number of positive (+) fluxes vs negative (-) fluxes as a ratio measured during the 2012 melt season GFC 7 is closest to the glacier in the perpendicular transect and n/d denotes no flux data for that sampling period due to the initial CO headspace concentration outside 200% of RG atmospheric concentrations.

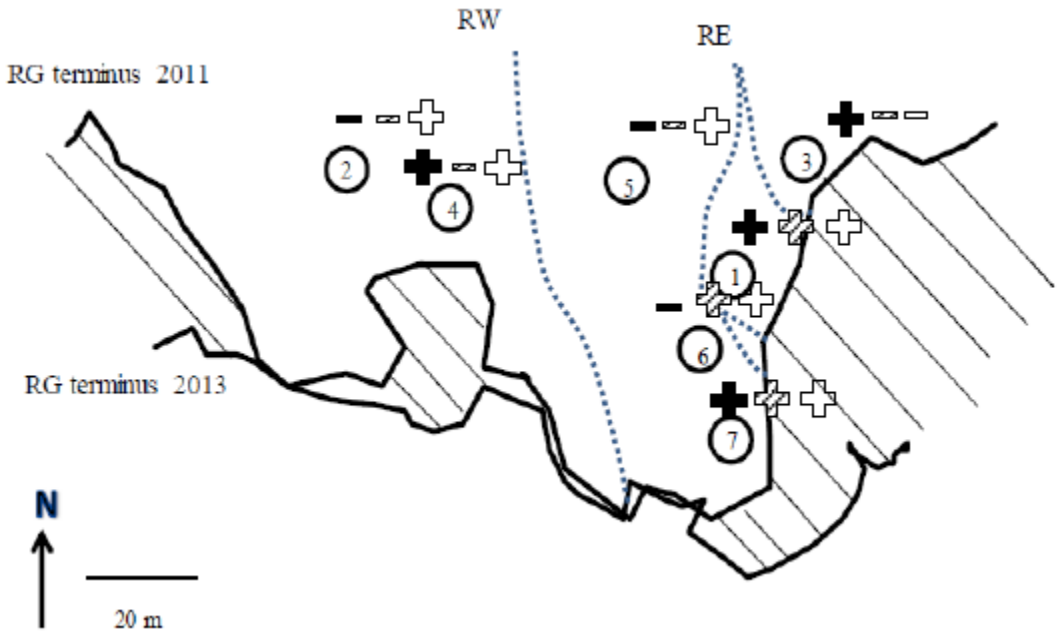

Figure 3.4. Schematic of the study area showing the locations where gas analyte fluxes were more positive than negative (as a plus sign) and where negative fluxes outnumbered the positive fluxes (as a negative sign). Filled signs are methane, hash marks are carbon dioxide and open signs are carbon monoxide.

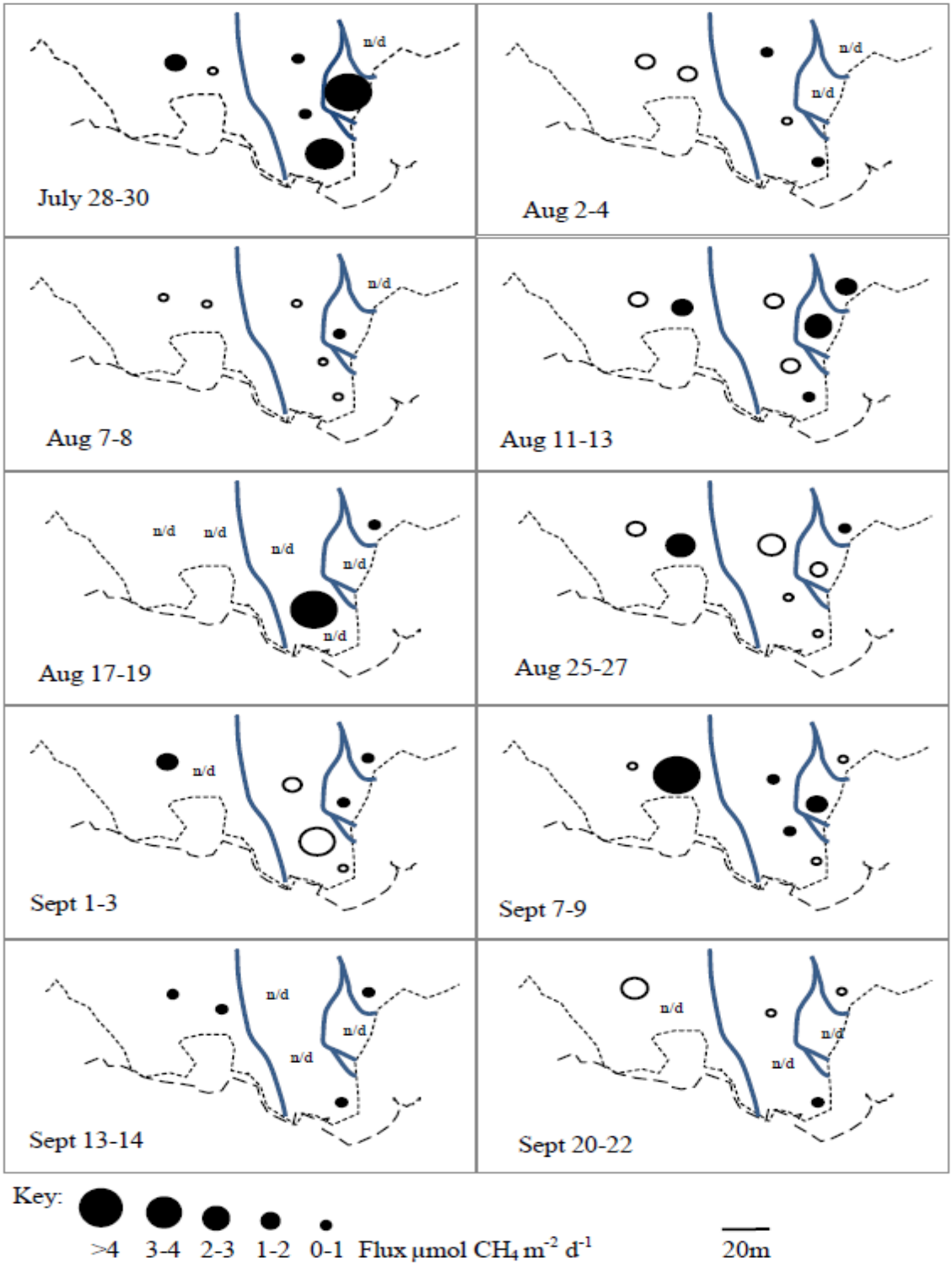

Figure 3.5. Spatial distribution and magnitude of methane fluxes during each sampling period. Long dashes are glacier terminus from 2012; short dashes are the terminus during 2011. Solid lines represent stream paths and n/d denotes no flux reported.

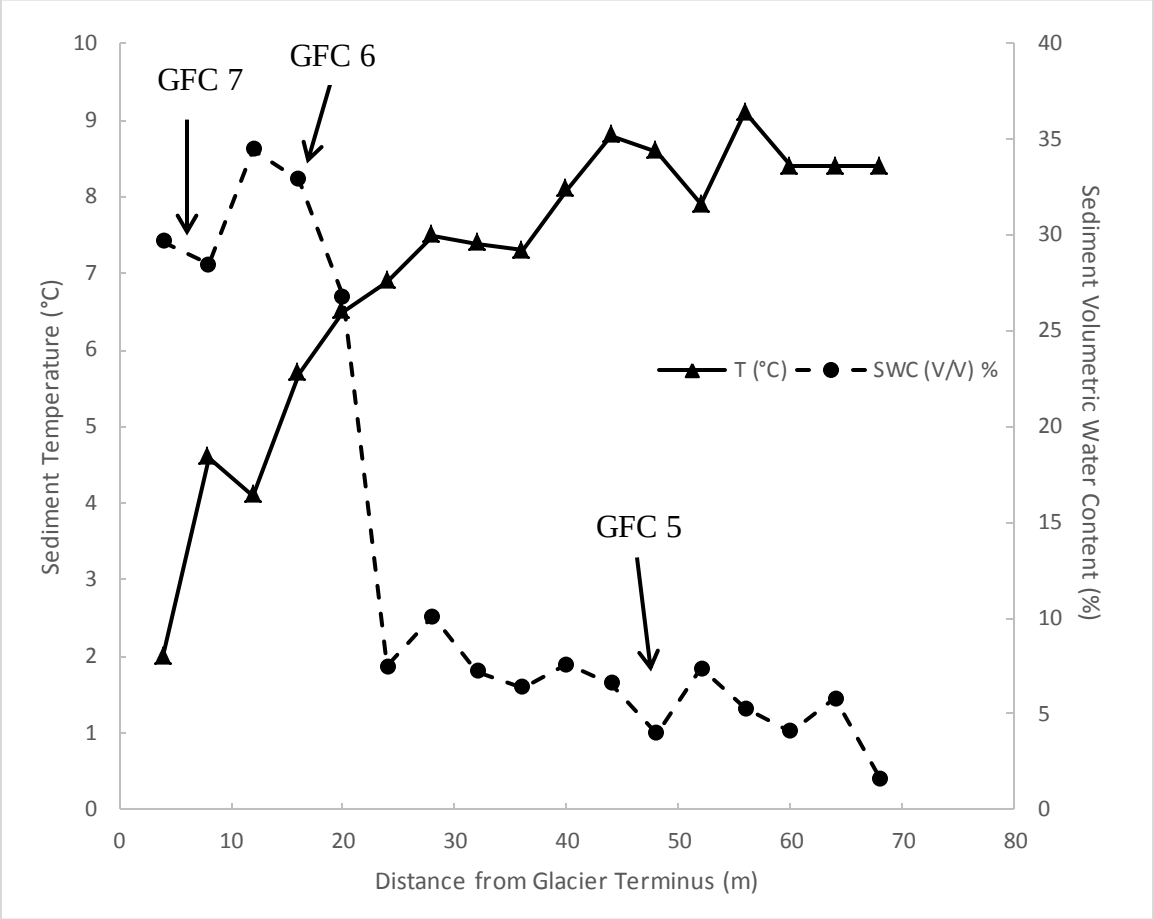

Figure 3.6. Sediment temperature and sediment volumetric water content along the sediment terrace measured at 12 cm depth, August 8th, 2013 with an Omega type E thermocouple and Campbell Hydrosense II, respectively. Water content decreases and sediment temperature increases, in general, with distance from the glacier terminus. The GFC locations denoted are relative to the approximate glacier terminus in September 2012. Notice the largest change in sediment water content occurs within 20 m of the terminus which would have included both GFCs 7 and 6 during 2012. Figure adapted from J. Dore, 2013 (not published).

3.1.3 Methane Flux Spatial and Temporal Statistical Analysis

One-way ANOVA statistical analysis was performed to determine any statistically significant sampling periods (temporal component) or gas flux chamber locations (spatial component). Specifically, spatial distribution analyses examined proximity to the glacier terminus (perpendicular transect: GFCs 5-7) along with a comparison of the average methane flux between all surface GFCs. The only statistically significant sampling period and GFC correspond to the highest measured flux.

The Mean Flux Across All GFCs Per Sampling Period There was strong evidence for statistically significant average fluxes for one sampling period relative to the melt season average flux (one way ANOVA, Case II[3], $\alpha = 0.05$); sampling period 1, July 28^{th}-30^{th}, (p-value = 0.003). The early season and late season average fluxes tended towards larger magnitudes with the middle of the melt season (August $7^{th} - 27^{th}$) revealing the lowest magnitude fluxes (see Figure 3.7).

Mean Flux Per GFC for All Sampling Periods The only GFC that was statistically significant from the average of the GFC melt season flux (one way ANOVA, Case II, $\alpha = 0.05$) was GFC 1 (p-value = 0.011). There was no evidence for a difference in mean methane fluxes between the three GFCs in the perpendicular transect (one way ANOVA, Case II, $\alpha = 0.05$) nor between the perpendicular and parallel transects (two sample t-test, $\alpha = 0.05$). Four of the seven GFCs had an average melt season flux of methane that was positive (Figure 3.8). GFCs 2, 5 and 6 exhibited negative average

[3] Case II refers to the case where individual group means are compared against an overall mean for all groups.

fluxes over the melt season and also had a cumulative melt season flux that was below zero (Figure 3.9). GFCs 1, 3, 4, and 7, GFCs closest to the glacier terminus (see Figure 2.2 for locations), all have a positive cumulative flux for the entire melt season. The sum of the cumulative fluxes for all the GFCs is 85.0 µmol m^{-2} over 57 days (2012 melt season).

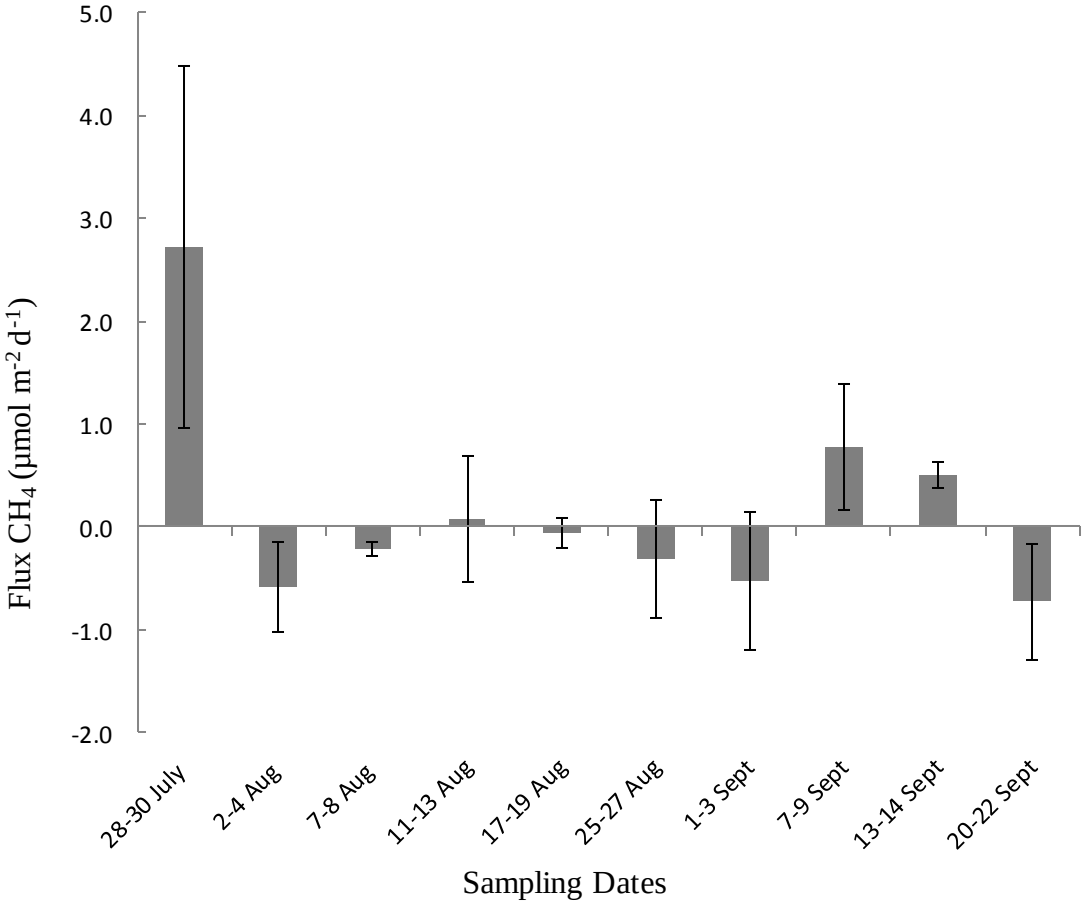

Figure 3.7. Mean flux of all GFCs for each sampling period. Error bars are standard error.

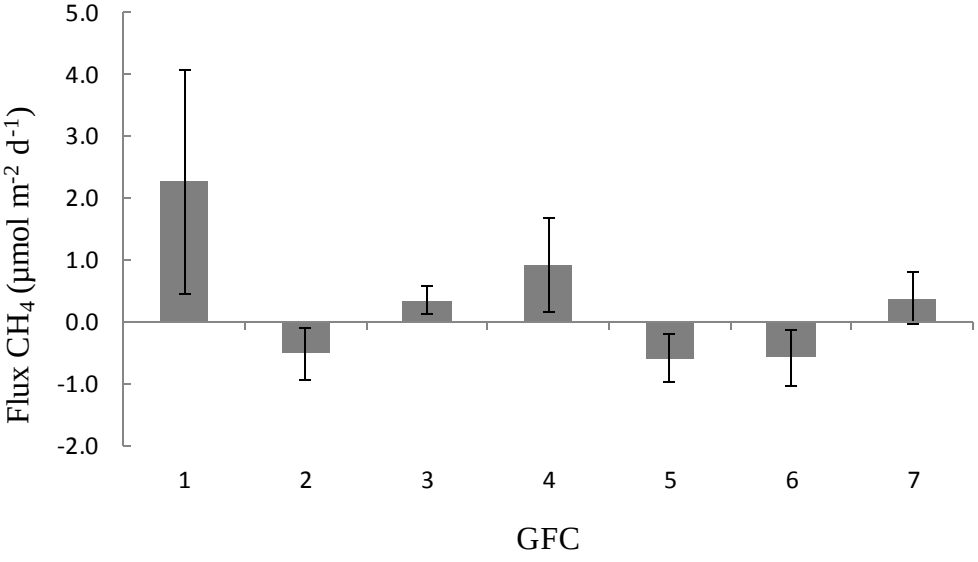

Figure 3.8. The mean flux for each gas flux chamber over the entire melt season. There is significant variability within each chamber (error bars are standard error).

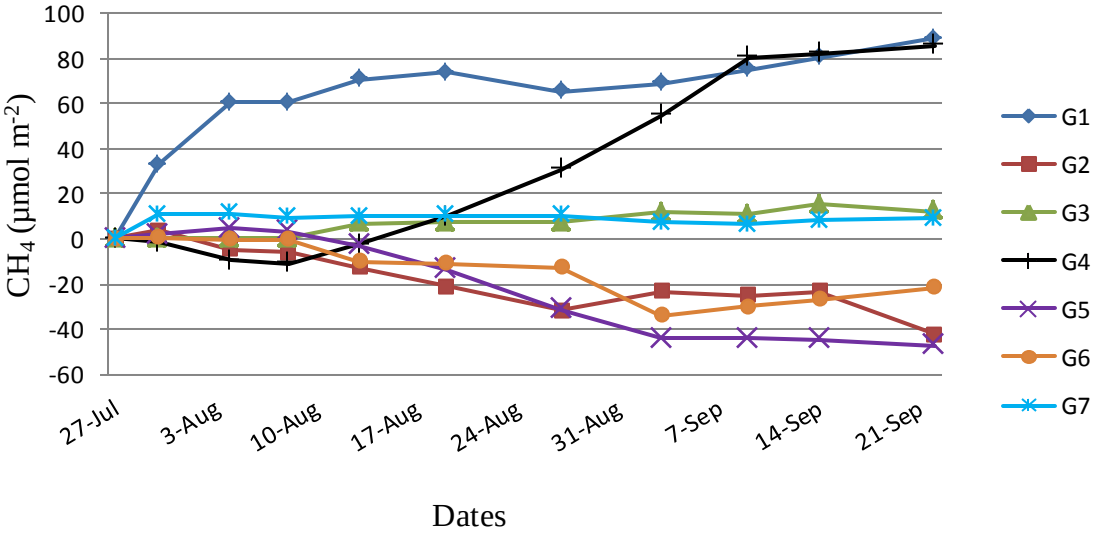

Figure 3.9. Cumulative melt season methane flux for each GFC. GFCs 2, 5, and 6 all have a cumulative value less than zero. If no flux was reported for a sampling period (SP) (see discussion in section 2.26) the two closest fluxes in time were averaged and used for that SP value. All fluxes start at zero as a function of the cumulative curve and it does not imply that a net flux of zero occurred on the 27th of July.

3.1.4 Methane Flux in GFC Depth Trio

The GFC depth chambers were intended to measure variations in flux, if any, at 5, 10, and 15 cm depths. The three depth chambers were located approximately 20 cm from each other so as to be comparable to one another. The depth trio was deployed at two different locations over the melt season. The CH_4 fluxes ranged from -5.9 to 6.4 µmol $CH_4\ m^{-2}\ d^{-1}$ in the depth chambers. The highest and lowest fluxes were measured at 15 cm and 5 cm, respectively. ANOVA statistical analysis revealed no statistical significance ($\alpha = 0.05$) between the gas flux chamber depths, 5, 10 and 15 cm implying that there was greater variability within each chamber than between the chambers over the entire melt season. Fluxes at location A (Figure 2.2) show a general decreasing in the strength of the flux with decreasing depth. However, location B (Figure 2.2), shows a different trend, with all chambers demonstrating a positive flux. A comparison of average fluxes between the two locations (see Figure 3.10) shows the largest magnitude fluxes at all depths occurred at location B during the latter part of the melt season (month of September).

3.1.5 Regression Analysis: Temperature, CO and CO_2 Gas Fluxes with the Flux of CH_4

CH_4 Flux and Sediment Temperature Sediment temperatures were recorded at every GFC while gas sampling. The reported values reflect the average subsurface temperature at a depth of 10 cm, measured with a soil temperature probe, for a given sampling period at each GFC. The correlation coefficients are relatively low for all linear

regressions ($r^2 < 0.35$ and p-values > 0.05 where $\alpha = 0.05$) implying little to no linear correlation between sediment temperature and the flux of methane (see Figures 3.11).

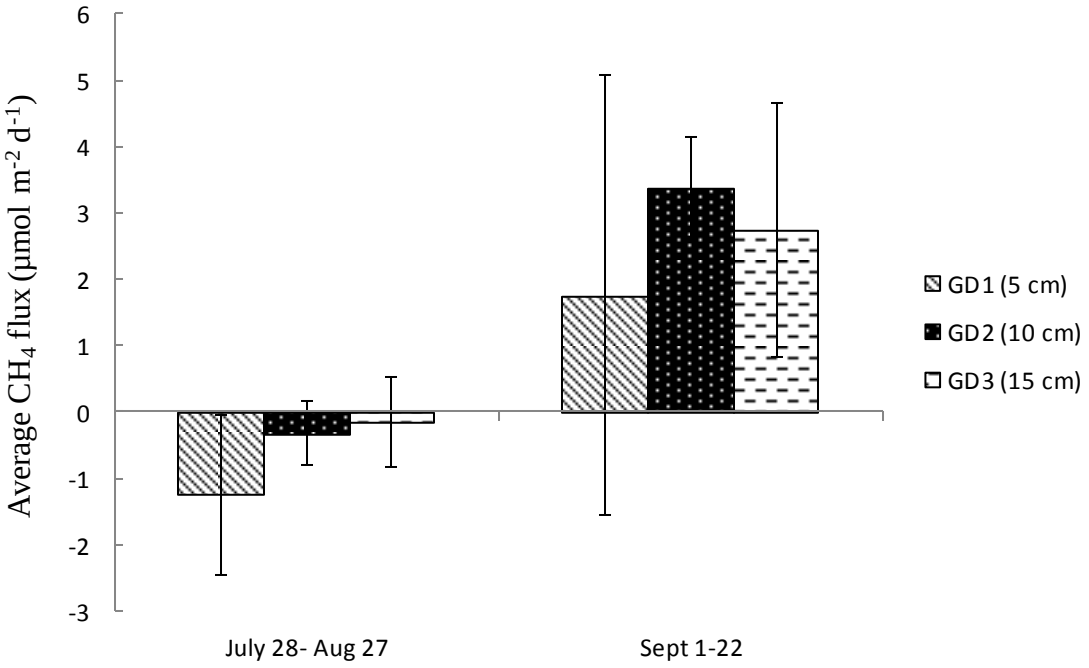

Figure 3.10. Depth chamber average fluxes compared between locations in the proglacial area. CH_4 fluxes were measured at location A from July 28th - August 27th and location B from September 1st - 22nd (see Figure 2.2 for locations). Values are the average fluxes for the sampling dates and error bars are standard error.

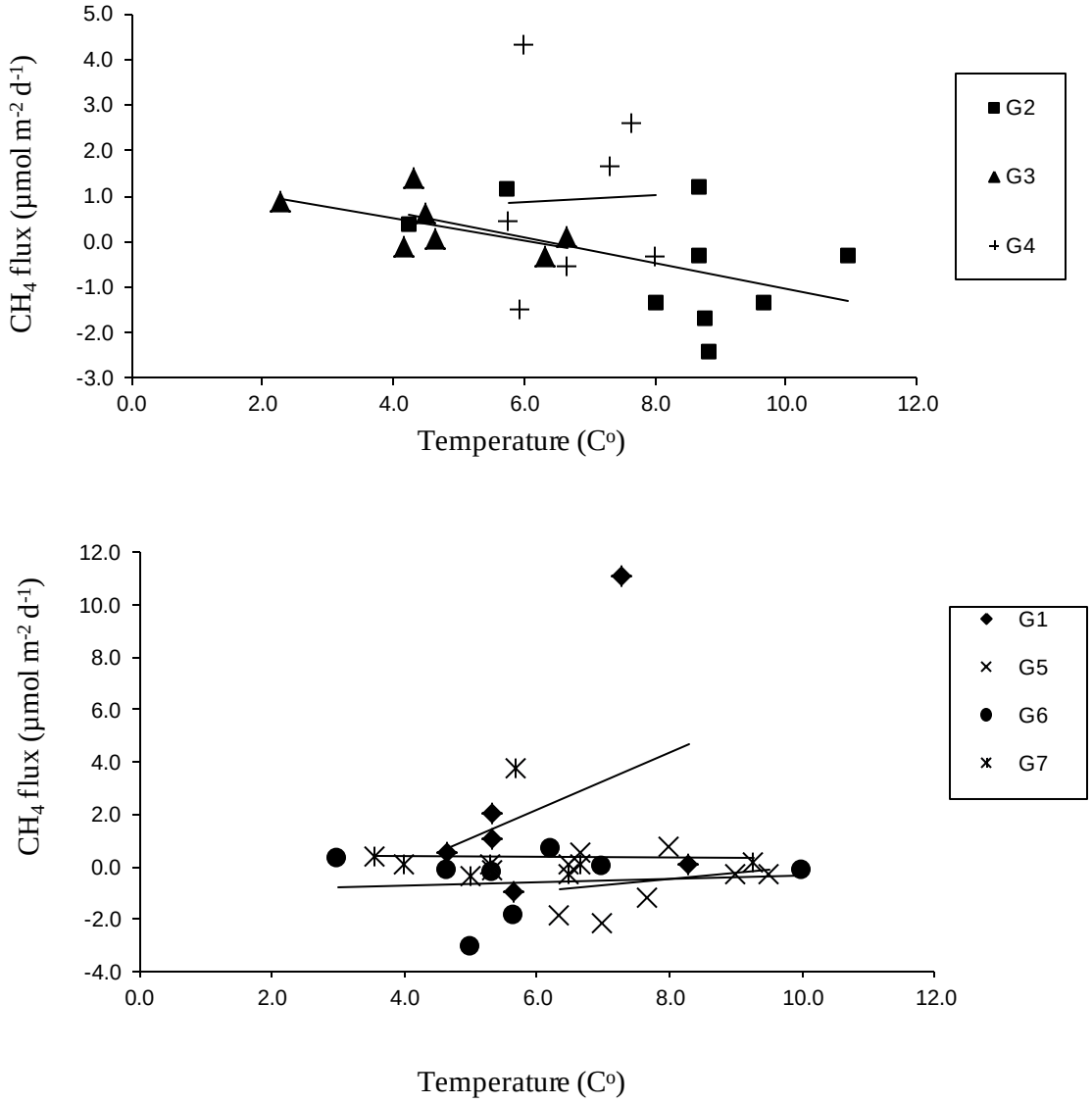

Figure 3.11. Linear regression analysis of sediment temperature and methane flux reveals no correlation (p-value > 0.05, $\alpha = 0.05$).

CH_4 Fluxes Compared with CO and CO_2 Gas Fluxes Methane and carbon monoxide were measured using the FID on the GC from the same gas sample and CO_2 was measured using the Vaisala CO_2 meter. The fluxes of the gases are reported in Appendix B and the relative flux magnitudes are presented in Figures 3.1-3.3. The associations between CO_2 and methane and CO and methane are, in general, weak and in opposition; CH_4 and CO_2 have a negative linear relationship and CH_4 and CO have a positive linear relationship (Figure 3.12). Linear regression analysis for all methane and CO fluxes are insignificant ($r^2 = 0.04$, p-value $= 0.22$, $\alpha = 0.05$, $n= 39$) as are the methane and CO_2 fluxes ($r^2 = 0.06$, p-value $= 0.99$, $\alpha = 0.05$, $n= 20$) from all GFCs per sampling period. Although there is no significant correlation between fluxes, the matrix and flux distribution figures (Figures 3.1-3.5) reveal that the surface GFCs closest to the glacier terminus on the sediment terrace reflect more positive fluxes for all gas analytes throughout the melt season. Whereas the surface GFCs located off the sediment terrace and near bedrock outcrops along the eastern and western edges, have more negative flux values over the melt season. The higher frequency of positive fluxes for all gases corresponds with the areas along the sediment terrace of greater water saturation.

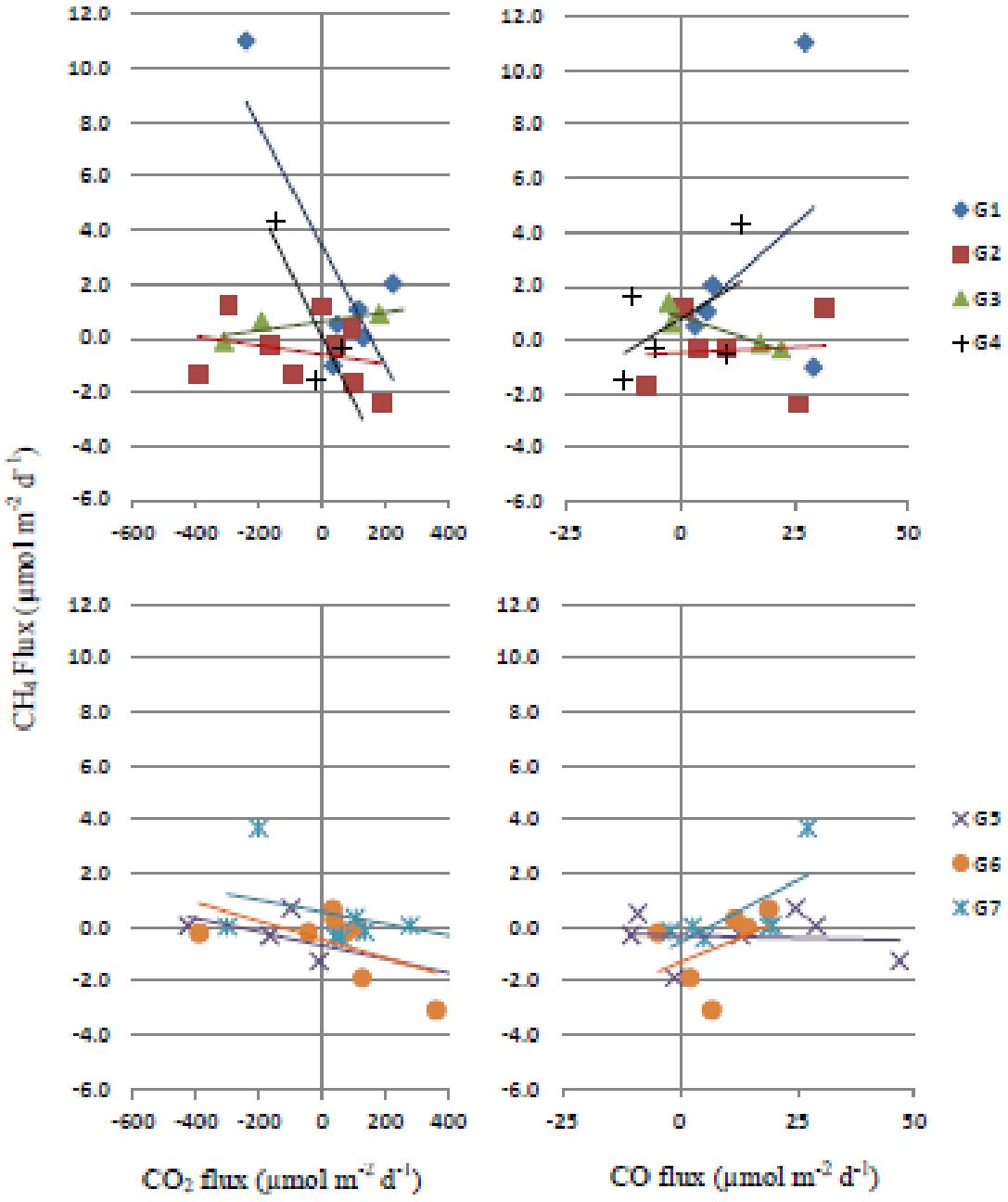

Figure 3.12. Methane fluxes compared to CO_2 (graphs on left) and CO fluxes (graphs on right) for each GFC during all sampling periods of the 2012 melt season.

3.2 Vertical Sediment Core Profiles

An analysis of four sediment cores, two from each field season, was conducted and included gas concentration (CO, CO_2, CH_4 and H_2) measurements and sediment characterization including porewater content, bulk volume, void volume, and particulate organic carbon content (POC). Cores A and B, collected July 11, 2011, were selected as representatives from a suite of five cores sampled within a meter of each other. Cores C and D, collected August 8 and September 8, 2012, respectively were selected based on contrasting locations; core C was off the sediment terrace further from the glacier terminus near a bedrock outcrop 15 m north of GFC 2 and core D was nearest the glacier terminus on the sediment terrace (see Figure 2.5 for coring locations). A vertical depth profile for each core was generated for gas analyte concentrations, porewater volume, and POC (Figures 3.13 and 3.14).

3.2.1 Sediment Core Gas Profiles

Gas profiles were generated for 4 sediment cores: A, B, C and D. The 2011 cores, A and B, were profiled for methane, carbon dioxide and carbon monoxide. The 2012 cores, C and D, were profiled for methane, carbon monoxide, carbon dioxide and hydrogen gas. Analysis for 2011 cores was conducted in November of 2012 and at this time the GC was not configured to measure low concentrations of H_2. During analysis of 2012 cores, conducted in May 2013, water was added to the samples to liberate gases. This may have affected the CO_2 measurements due to potential carbonate mineral dissolution, however, CO_2 data is still included in the results for the 2012 cores as

analysis of this method revealed less than a 20% decrease in the headspace concentrations before and after the addition of water to the sample. The core profiles show the concentration of analytes per subsample bulk volume as an average of puck triplicates in units of nmol cm^{-3}. Methane concentrations across the cores ranged from 0.85-20.71 nmol cm^{-3}. While the depth of peak concentration varied between cores, each core demonstrated at least one subsurface peak in methane concentration with the highest concentrations occurring within 4 cm of the surface. Carbon monoxide concentrations ranged from 0.14 – 0.71 nmol cm^{-3}. All measurable concentrations of CO exceeded atmospheric concentration (0.004 nmol cm^{-3}) which would be below the detection limit of the FID (0.04 nmol CO cm^{-3}). There were several depths where no CO was measured, either it was below detection limit or not present. Hydrogen gas ranged from 0.19 – 0.89 nmol cm^{-3} with all reported values higher than atmospheric concentrations (0.024 nmol cm^{-3}) which were also below GC detection limit (0.04 nmol H_2 cm^{-3}). Carbon dioxide concentrations ranged from 12 – 427 nmol cm^{-3} with the highest concentrations occuring within the shallowest depths adjacent to the sediment surface (see Table 3.2 for all reported average gas analyte values and one standard deviation).

3.2.2 Sediment Core Porosity, Porewater and Particulate Organic Carbon Content

Porosity was calculated as the volume of voids (equal to volume of porewater, see discussion in 3.1.7) per bulk volume of each subsample and triplicate subsamples were averaged for overall puck porosity. This porosity measure is likely an underestimate as it assumes 100% water saturation and results in a gas analyte concentration underestimate

also. The range of porosity across cores was 0.10-0.77 with an average of 0.20 ± 0.14 (1σ). The shallowest section of core B had the highest porosity (0.77) which was attributed to the presence of an ice lens in this sample. Removal of this outlier results in an average porosity of 0.17 ± 0.05 (1σ) and a significant reduction in the coefficient of variance (CV); 70% to 29%.

The average percent porewater per puck was 10.6 wt % ± 11.6 % (1σ) of wet sediment. Again the removal of the outlier value in the upper most section of core B changes the average percent porewater to 8.1 % wt ± 2.8% (1σ) and the CV from 110% to 35%. POC per puck was 1.77 wt % ± 0.55 % (1σ) of dry sediment where cores B, C and D all have < 2% organic carbon (OC) by dry sediment weight and core A has 2-3% OC by weight at all depths.

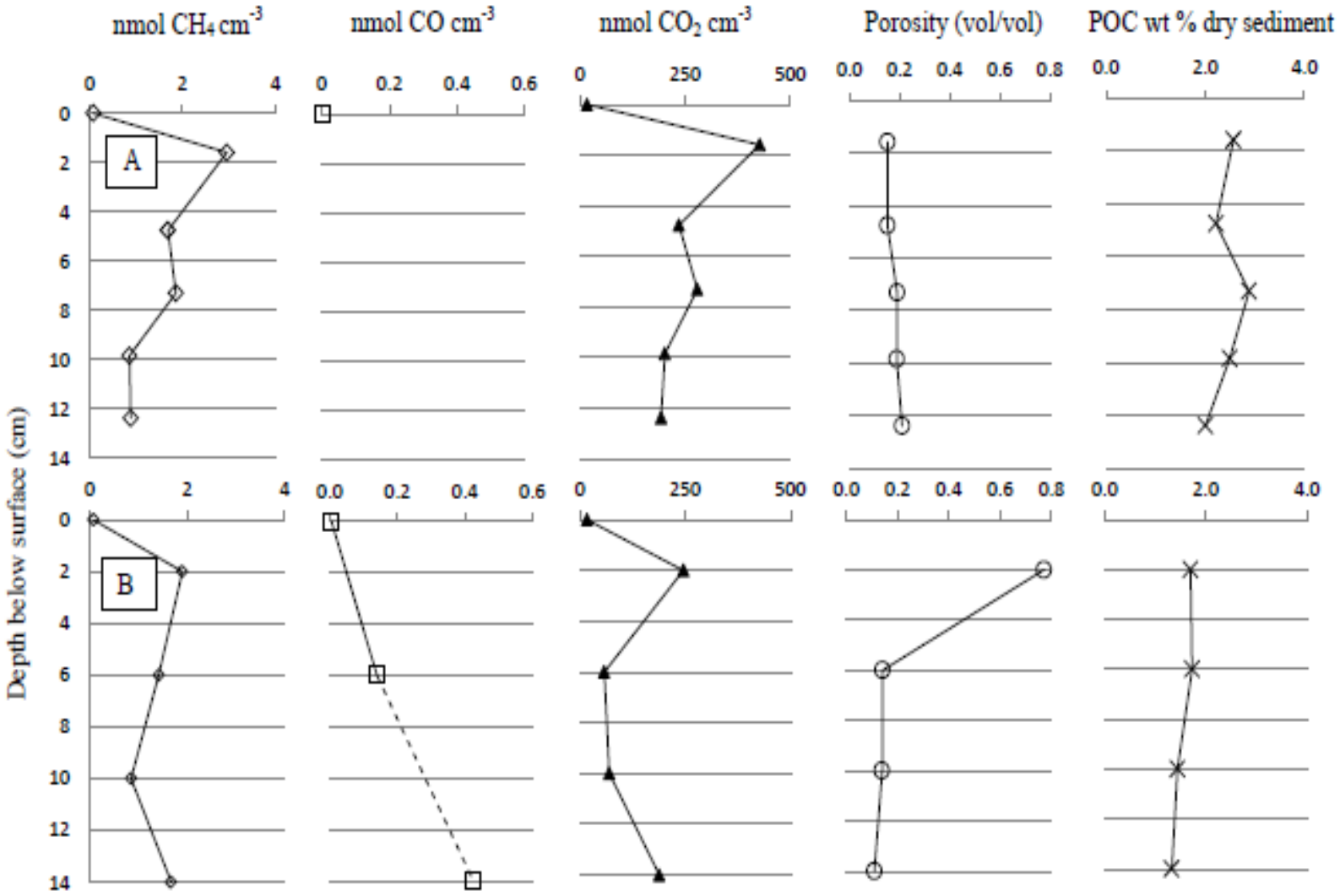

Figure 3.13. Vertical sediment core profiles from 2011 field season. All plotted points represent the midpoint of a vertical sample section. 2011 cores were not sampled in triplicate. Dotted lines denote areas where data was discontinuous in the profile. The porosity is the ratio of void volume to wet sediment volume where the porewater volume equals the volume of voids.

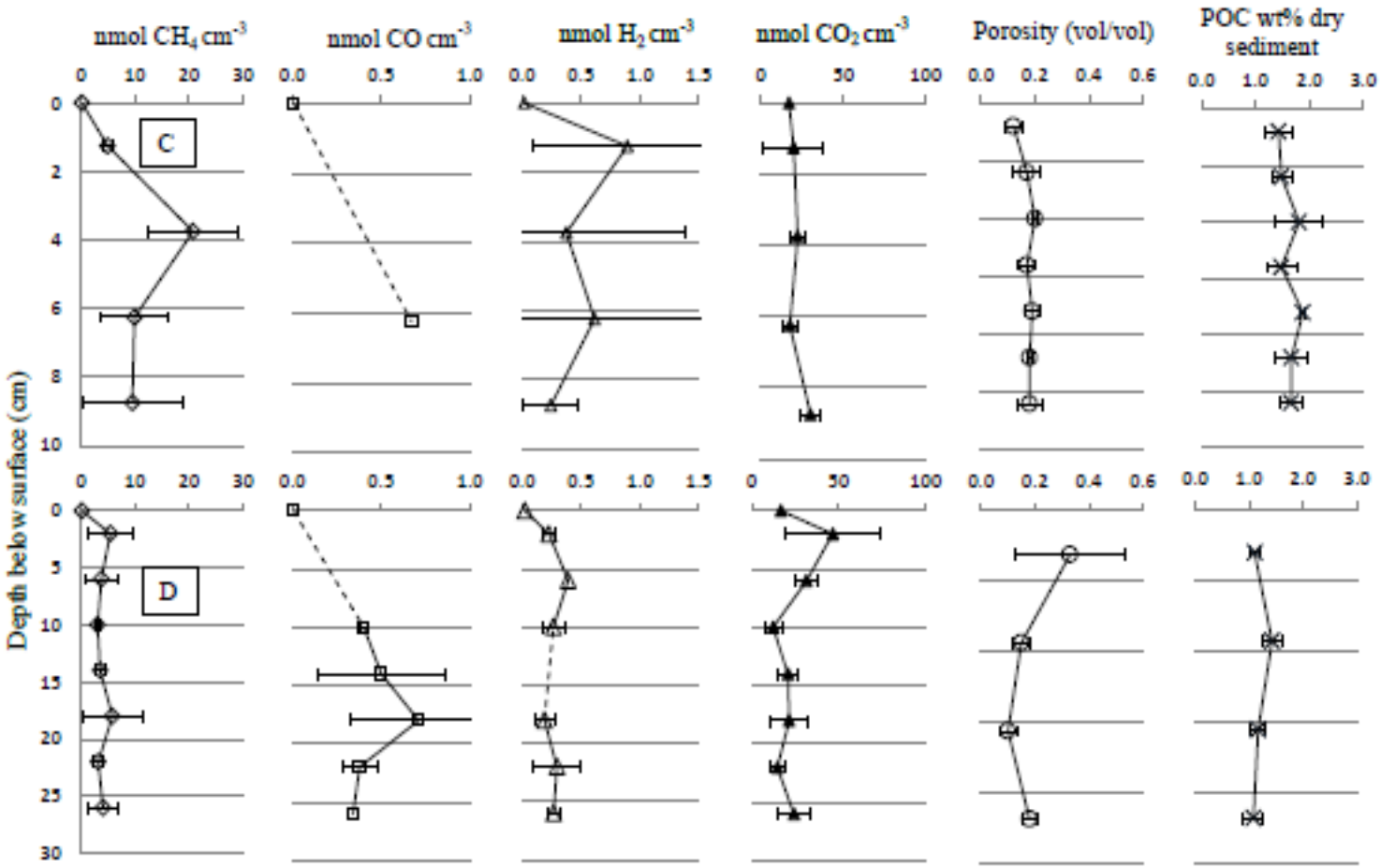

Figure 3.14. Vertical sediment core profiles from 2012 field season. Notice the vertical axes are different, core C was 10 cm in depth and core D was 28 cm in depth. All plotted points represent the midpoint of a vertical sample section. 2012 cores were sampled in triplicate and data is the average value of triplicates and error bars are one standard deviation. Dotted lines denote areas where data was discontinuous in the profile. If no error bars are present there was only one triplicate sample that was not below the detection limit. The porosity is the ratio of void volume to wet sediment volume where the porewater volume equals the volume of voids. The high porosity in core C at 1.5 cm is the result of a visible ice lens contributing to the overall void volume.

Table 3.2. Average nmol cm^{-3} per gas analyte and one standard deviation reported for all measured depths within cores. Atmospheric concentrations listed for comparison.

Core	Depth (cm)	CH_4	σ	CO	σ	H_2	σ	CO_2	σ
Atmospheric		0.08		0.004		0.02		16.86	
A*	0-3.2	2.95	-	bdl**		n/a+		426.92	-
	3.2-5.7	1.68	-	bdl		n/a		234.96	-
	5.7-8.3	1.86	-	bdl		n/a		278.69	-
	8.3-10.8	0.86	-	bdl		n/a		201.64	-
	10.8-13.3	0.88	-	bdl		n/a		192.62	-
B*	0-4	1.90	-	bdl		n/a		245.87	-
	4-8	1.42	-	0.14	-	n/a		57.62	-
	8-12	0.85	-	bdl		n/a		69.48	-
	12-16	1.67	-	0.43	-	n/a		188.70	-
C	0-2.5	4.87	0.80	bdl		0.89	0.80	19.61	18.06
	2.5-5	20.71	8.43	bdl		0.38	1.01	22.18	4.20
	5-7.5	9.85	6.15	0.67	-	0.61	1.05	17.42	4.92
	7.5-10	9.45	9.19	bdl		0.24	0.23	29.93	6.38
D	0-4	5.34	4.21	bdl		0.23	0.06	46.58	26.58
	4-8	3.69	3.08	bdl		0.39	-	31.53	6.91
	8-12	2.99	0.53	0.40	0.02	0.26	0.09	12.42	5.07
	12-16	3.46	1.08	0.50	0.36	bdl		20.95	5.65
	16-20	5.72	5.62	0.71	0.38	0.19	0.08	21.59	10.97
	20-24	3.12	0.95	0.38	0.10	0.30	0.20	14.81	3.88
	24-28	3.97	2.82	0.34	-	0.27	0.06	24.41	9.53

*2011 cores were not run in triplicate and H_2 not analyzed.

** denotes values below detection limit

+ n/a denotes analytes not analyzed

- Only one data point therefore no standard deviation value reported

3.2.3 Statistical Analysis of Physical Parameter Correlations with Methane Concentration

Regression analysis for 2011 core data reveals a strong correlation ($\alpha = 0.05$) between the concentrations of methane and carbon dioxide ($r^2 = 0.64$, $p = < 0.01$, $n = 9$), but collective (2011 and 2012) core data results in little to no correlation ($r^2 = 0.16$, $p = 0.08$, $n = 20$). While the linear correlation is not strong (based on $r^2 \geq 0.5$) a significant correlation exists between methane concentrations and organic carbon content for the collective 2011 and 2012 core data ($r^2 = 0.19$, $p = 0.05$, $n= 20$). Other potential explanatory variables, carbon monoxide and hydrogen concentrations, percent porewater and porosity, had insignificant relationships ($p > 0.05$) with the concentrations of methane in the cores (see Table 3.3 for all r^2 values, sample sizes and p-values and Figure 3.15 for linear regression plots).

Regression analysis for individual cores reveals, in some circumstances, stronger correlations than collective core data. There is a strong linear correlation between CO_2 concentrations and methane concentrations for the 2011 cores ($r^2 = 0.94$, p-value < 0.01; $r^2 = 0.64$, p-value $= 0.17$ for cores A and B, respectively). Also, there is a weak linear correlation between the concentration of methane and percent porewater for all cores ($r^2 \geq 0.23$, p-values > 0.05). There is little to no linear correlation between methane and carbon monoxide concentrations ($r^2 \leq 0.09$, $p > 0.7$) and core C methane concentrations have a linear correlation to % POC ($r^2 = 0.89$, p-value $= 0.06$).

Table 3.3. Linear regression analysis r^2 values, sample size (n) and p-values (p) where $\alpha = 0.05$ for collective core data and individual cores. POC is the particulate organic carbon as a percent of dry sediment weight, PW is the average porewater as a percent of wet sediment weight and gas units are nmol cm^{-3}. Hydrogen gas was not analyzed in cores A and B and no CO was detected in core A (denoted by n/a).

	CH_4 vs POC			CH_4 vs PW			CH_4 vs CO_2			CH_4 vs CO			CH_4 vs H_2		
	n	r^2	p	n	r^2	p	n	r^2	p	n	r^2	p	n	r^2	p
All Cores	20	0.19	0.05	20	0.02	0.54	20	0.16	0.08	20	0.004	0.78	11	0.03	0.63
Core															
A	5	<0.1	0.90	5	0.55	0.15	5	0.94	<0.01	n./a	n/a	n/a	n/a	n/a	n/a
B	4	0.08	072	4	0.40	0.36	4	0.69	0.17	4	0.10	0.69	n/a	n/a	n/a
C	4	0.89	0.06	4	0.34	0.41	4	<0.1	0.92	4	0.02	0.86	4	0.33	0.42
D	7	<0.1	0.92	7	0.23	0.27	7	0.37	0.15	7	<0.1	0.89	7	0.01	0.81

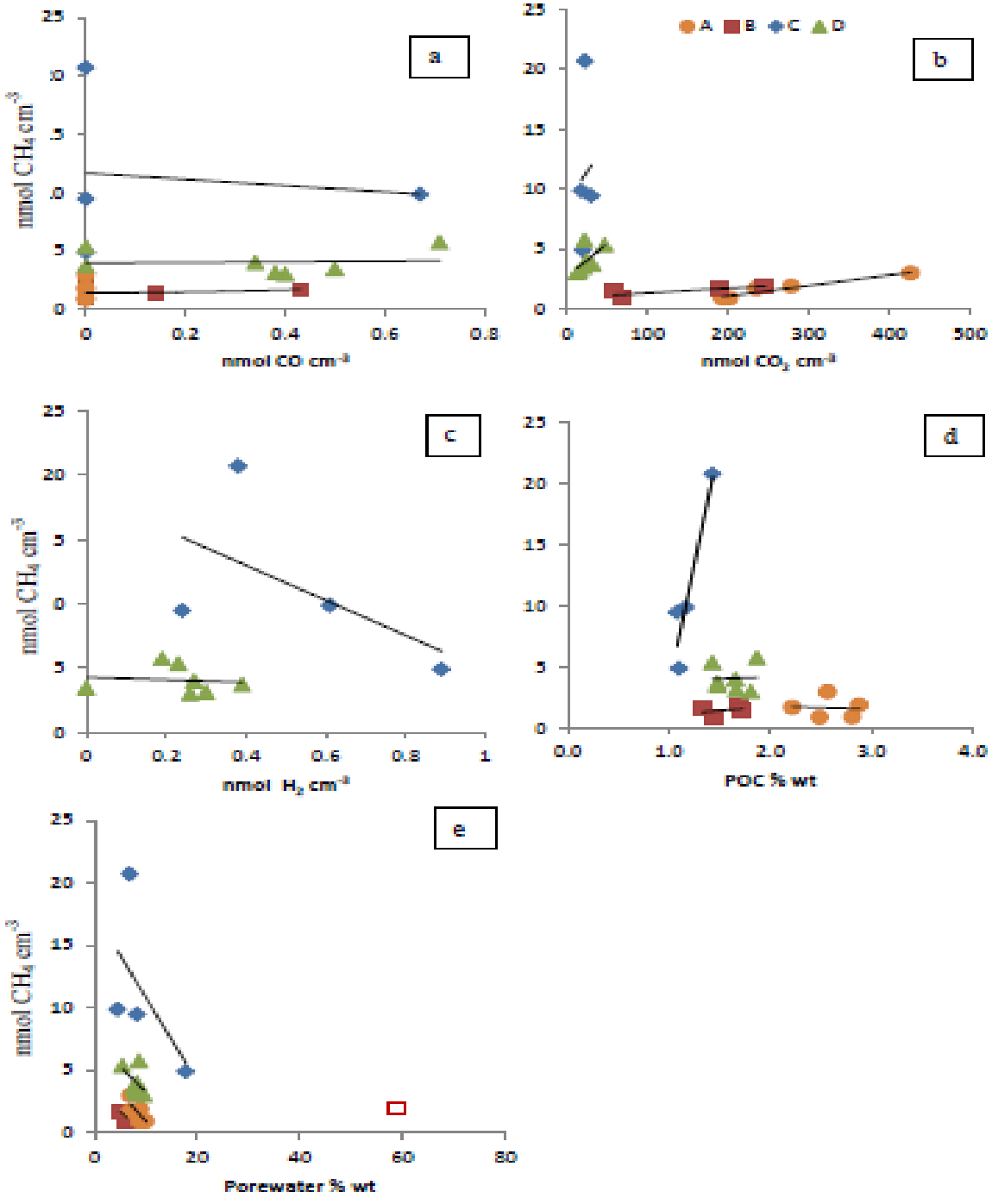

Figure 3.15. Linear regression plots for individual core methane concentrations and concentrations of a) CO, b) CO_2, c) H_2, d) POC, and e) porewater. The red box in graph e is an outlier for Core B.

3.2.4 Diffusive Methane Flux

A steady state flux, *J*, was calculated for each core based on Fick's first law:

$$J = D_{eff}(\frac{dC}{dz}) \qquad \text{(Eq 3.7)}$$

where *dC* is the difference in gas concentrations at depths z_1 and z_2, and *dz* is the difference between z_1 and z_2. The depths and concentrations used in determining the flux reflect the flux of gas analyte from the uppermost portion (generally within 4 cm) of the sediment core to the surface. The effective diffusion rate, D_{eff}, is the diffusivity of CH_4 based on the water-induced linear reduction (WLR) model (Moldrup et al., 2001). The WLR model considers the effect of water in pore spaces on the diffusion of gas. The greater the air filled porosity, the lower the water content and the greater is the diffusivity of gas due to less impedance by water.

$$D_{eff} = D_o(\varepsilon^{1.5})\frac{\varepsilon}{\phi} \qquad \text{(Eq 3.8)}$$

The free air diffusion coefficients (based on algorithm from Tucker and Nelken (1982)), D_o, for each analyte is D_{CH4} = 2.47 x 10^{-5} m^2 s^{-1}, D_{CO2} = 1.82 x 10^{-5} m^2 s^{-1} and D_{CO} = 2.18 x 10^{-5} m^2 s^{-1} all at T = 277°K and P = 0.75 atm, ε is the air-filled porosity and ϕ is porosity.

$$\varepsilon = V_{air\,filled\,voids}/V_{bulk} \qquad \text{(Eq 3.9)}$$

and

$$\phi = V_{voids}/V_{bulk} \qquad \text{(Eq 3.10)}$$

Diffusive fluxes assume isobaric and isothermal conditions at depth. Fluxes were calculated based on a 0%, 90% and 99% water saturation of void volume. From visual field observations the sediments near the surface experience high variability in water saturation over the course of the melt season. Initially, seasonal snow melt dominated, followed by glacial ice melt and stream channels, supraglacially, subglacially and in the proglacial area became more defined during the melt season. Melt diminished as the melt season reached its end in September, accompanied by a rapid decrease in stream discharge. This seasonal hydrological development affected the degree of sediment saturation proximal to the sources of water. Wetting and drying cycles will have a significant influence on the efflux of gas (Scanlon et al., 2001). Calculated minimum (99% saturation) and maximum (0% saturation) flux values provide constraints on the potential flux of methane, carbon dioxide and carbon monoxide from the sediments to the atmosphere.

Table 3.4. Diffusive gas fluxes (*J*) based on 99%, 90 %, 50% and 0% water saturation of void volume. Positive fluxes imply an efflux or transport of gas analyte from sediment to atmosphere via molecular diffusion. Core A carbon monoxide values were all below detection limit so the diffusive gradient is from atmospheric concentrations to zero in the uppermost portion of the core. The measured flux from the nearest GFC on the date of core collection is listed for comparison. Note that these flux values are minimum estimates as the porosity is a minimum value (see discussion in 2.3.5).

Core and analyte	*J* (μmol m^{-2} d^{-1})				
	99% saturation	90% saturation	50% saturation	0% saturation	Nearest GFC
A					
CH_4	0.11	3.63×10^{1}	2.03×10^{3}	1.15×10^{4}	8.31
CO	-1.30×10^{-4}	-4.10×10^{-2}	-2.29	-1.30×10^{1}	-
CO_2	1.45×10^{1}	4.58×10^{3}	2.56×10^{5}	1.45×10^{6}	-
B					
CH_4	0.72	2.08×10^{2}	5.82×10^{3}	6.58×10^{4}	8.31
CO	1.04×10^{-2}	3.09	2.50×10^{1}	9.79×10^{2}	-
CO_2	8.39×10^{1}	2.31×10^{4}	1.29×10^{6}	7.31×10^{6}	-
C					
CH_4	0.78	2.45×10^{2}	1.37×10^{4}	7.75×10^{4}	-0.16
CO	1.60×10^{-2}	4.93	2.76×10^{2}	1.56×10^{3}	-1.92
CO_2	1.78	5.62×10^{2}	3.14×10^{4}	1.78×10^{5}	135.58
D					
CH_4	0.12	3.69×10^{1}	2.06×10^{3}	1.17×10^{4}	-0.30
CO	4.00×10^{-3}	1.32	7.37×10^{1}	4.17×10^{2}	4.04
CO_2	2.63	8.33×10^{2}	4.67×10^{4}	2.63×10^{5}	40.26

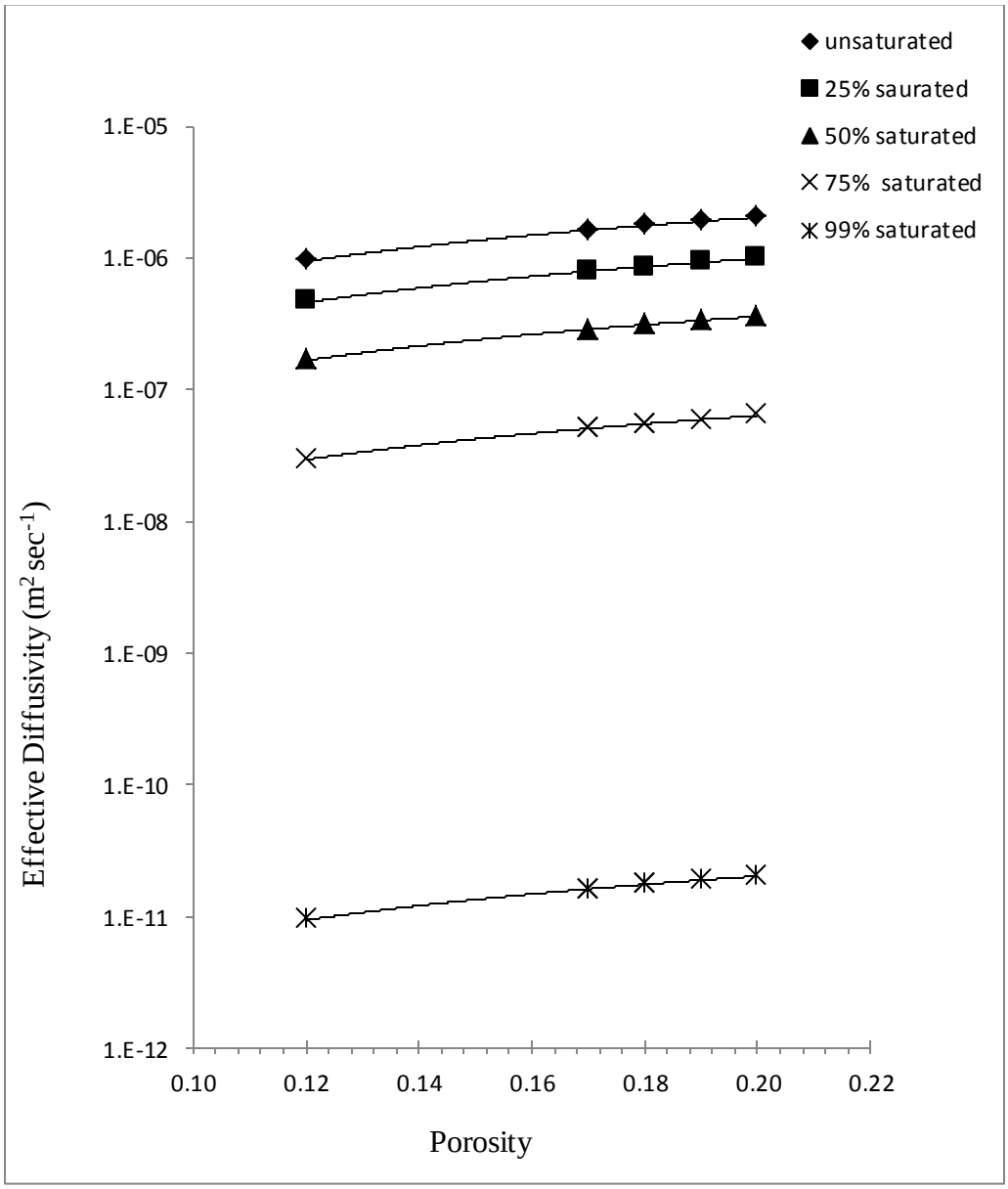

Figure 3.16. Diffusivity curves based on core D porosity data calculated for each puck and various percent saturations. The increase in diffusivity of CH_4 coincides with an increase of porosity at low saturation. With increasing saturation, diffusivity of gas is less dependent on the porosity. Note the log scale on the y-axis.

CHAPTER 4 - DISCUSSION

There is evidence that methanogens and methanotrophs are present in glacial sediments (Barcena et al., 2010; Boyd et al., 2010; Nauer et al., 2012; Hamilton et al., 2013). A quantifiable efflux of methane from the sediments to the atmosphere would indicate a subsurface source of methane. Factors affecting the efflux may be related to microbial parameters (i.e. methane oxidation via methanotrophy or rates of methanogenesis) or physical parameters (i.e. sediment temperature, water saturation, effective porosity). This study evaluated the physical parameters.

Methane concentrations were measured from samples collected from gas flux chambers, placed on the sediment surface, in transects both parallel to and perpendicular to the glacier terminus. Measurements were made over a melt season, July to September 2012, and used to determine both spatial and temporal variability in the methane flux at this retreating, temperate glacier. During 10 sampling periods, over 300 gas samples were collected and analyzed from 10 different gas flux chamber locations in the proglacial area within 50 m of the glacier terminus. Previous experiments in Greenland and the Swiss Alps (e.g. Barcena et al., 2010 and Nauer et al., 2012, respectively) relied on single sampling periods from which net methane fluxes from the sediments to the atmosphere were calculated. While addressing the spatial variability of the methane flux these studies do not address temporal variations in the flux of methane during a melt season. The data set in this study indicates the flux of gases from glacial sediments is highly variable both spatially and temporally indicating that single sample periods may either over or underestimate the average melt season methane flux from a glacial system.

Shallow sediment cores, collected adjacent to the static chambers were used to generate vertical sediment profiles of gas concentrations, porosity, water content, and particulate organic carbon (POC). Methane concentrations were higher than atmospheric in all cases within the profiles indicating a source of methane at depth in the sediments. Linkages between core profile methane concentrations and net methane fluxes are discussed based on diffusion and potential biogeochemical processes in the sediments. Understanding the processes and variables that impact the net flux of methane from glacial sediments may help to constrain modeling studies simulating the impacts of methane from glacial systems on global methane budgets.

4.1 Methane Fluxes: Temporal and Spatial Variability

4.1.1 Surface Methane Flux

The concentration of methane, measured in gas flux chamber headspace, changed over time during the 2012 field season from July 28th to September 22nd. The mean methane concentration of all GFCs at each time point, T_0, T_1 and T_2 (corresponding to time 0, 24 and 48 hours, respectively) for all the sampling periods revealed a gradual increase (5.6% of the original T_0 value) over the 48 hour sampling period. Surface fluxes ranged from -3.08 to 11.02 μmol CH_4 m^{-2} d^{-1} with an overall average surface flux of 0.22 ± 0.27μmol CH_4 m^{-2} d^{-1} (n = 54) during the 2012 field season (July 28th –September 22nd). The early and late season fluxes, in general, are larger in magnitude and more variable than the mid season fluxes (refer to Figure 3.7). This temporal division may reflect physical changes in the proglacial sediments over the course of the melt season and/or changes in microbial community populations or their activity.

The higher frequency of negative fluxes distally from the glacier terminus, as seen in GFCs 2 and 5 (see Figure 3.4), suggests that sediments further from the glacier, with longer exposure to atmospheric conditions, may potentially act as a methane sink through the oxidation of methane. A similar finding was also reported by Barcena et al. (2010) in the forefield of Mittivakkat Glacier in Greenland where methane oxidation potential increased with distance from the terminus and the only GFC with a positive flux (0.44 µmol CH_4 m^{-2} d^{-1}) to the atmosphere was within 1 m of the glacier terminus and the next closest chamber was ~ 80 m from the glacier terminus. This trend suggests that proximity to the glacier affects the methane flux. Such effects are likely the result of changes in the proglacial sediments including sediment temperature, water content which affects the diffusion of gases from the sediments and the diffusion of oxygen (generating an anoxic environment) and microbial community structure since the time of glacial retreat.

4.1.2 Subsurface Methane Fluxes

Methane fluxes measured in the depth GFCs (5, 10 and 15 cm below surface) ranged from -5.9 to 6.4 µmol CH_4 m^{-2} d^{-1}. Location A, July 28th to August 27th, was near GFC 1 on the southeastern edge of the sediment terrace and had been exposed since at least 2011. Fluxes measured at location A were negative demonstrating a decreasing magnitude with decreasing depth potentially indicating that the glacial sediments are acting as a sink due to microbial activity at depth. Location B, was in saturated sediments that were uncovered by retreat of the glacier terminus during the 2012 melt season. At location B, the mean fluxes show a strong positive flux at 5, 10 and 15 cm

with the highest flux occurring at 10 cm: 1.8 µmol CH_4 m^{-2} d^{-1} (5 cm), 3.4 µmol CH_4 m^{-2} d^{-1} (10 cm) and 2.7 µmol CH_4 m^{-2} d^{-1} (15 cm) (see Figure 3.10). This may indicate a methane source at 10 cm depth that is a) diffusing up and downward and/or b) methanotrophic activity is potentially decreasing the flux at the other depths.

4.1.3 CO Surface Gas Fluxes

No significant correlations were observed between the sediment temperature (10 cm depth), CO and CO_2 gas fluxes and the measured flux of methane at each GFC throughout the melt season (refer to Figures 3.11 and 3.12). However, a strong efflux of carbon monoxide from the glacial sediments was observed. While the concentrations of methane and carbon dioxide in the RG ambient air, sampled ~ 1 m above the sediment surface, remained relatively constant over the course of the 2012 field season, carbon monoxide concentrations increased from 0.8 ppmv to 3.2 ppmv over the field season, a value 32 times greater than the global average carbon monoxide concentration of 0.1 ppmv (Conrad, 1996). The GFC initial, T_0, headspace concentrations were higher than atmospheric during almost every sampling period and also reflect an increased carbon monoxide concentration at the end of the 2012 melt season. Early season (July 16th – September 7th) T_0 concentrations ranged from 0.2 - 6.4 ppmv with a mean of 2.1 ± 1.5 ppmv (n = 58). While later season (September 13th –September 20th) T_0 concentrations ranged from 4.9-12.1 ppmv with a mean of 8.3 ± 0.5 ppmv (n = 14). This fourfold increase in both the average GFC headspace and the average ambient air CO concentrations indicates an increase in the CO source within the sediments or a decrease in the consumption rate of CO. Potential sources of carbon monoxide, methane and

carbon dioxide are discussed further below. The high variability in fluxes, both spatially and temporally, is not uncharacteristic of soil-atmosphere gas fluxes (Conrad, 1996). The gas fluxes are likely modulated to some degree by microbial activity and the microbial community would be under pressure to adapt to changing physical conditions within the glacial sediments (Kotsyurbenko, 2005). Changing conditions in temperature, substrate, and oxidant availability could either inhibit or encourage certain members of the microbial community resulting in variable fluxes of products (i.e. methane and CO_2) within the sediments and ultimately to the atmosphere. Potential sources, both biotic and abiotic, of the gas analytes are discussed further in relation to the results of this research.

4.2 Heterogeneous Concentrations of Gases in Vertical Sediment Core Profiles

Four sediment cores, ranging from 10 to 30 cm in depth were profiled for CH_4, CO, CO_2 and H_2 gas analytes, porewater content, bulk and void volumes and particulate organic carbon content (see Figures 3.13 and 3.14). Each core shows a high degree of variability in gas analytes; CH_4, CO, CO_2 and H_2, within the vertical sediment profiles. Following is an analysis of the potential metabolic pathways utilized by the putative subglacial microbial consortia previously demonstrated in RG sediments (Boyd et al., 2011; Boyd et al., 2010; Hamilton et al., 2013). Boyd et al. (2010) documented biomarker evidence for methanogens in RG sediments, including the presence of coenzyme M, GDGT-O lipids, Archaeal 16S rRNA gene sequences, *mcrA* gene sequences and methane concentrations in equilibrium with porewater up to 29 ppmv (similar to results of this research). More recently, Hamilton et al. (2013) found that 95%

95% of the Archaeal community in RG subglacial sediments were methanogens, specifically from the orders *Methanomicrobiales* and *Methanosarcinales*. RNA-based approaches, such as were used by Hamilton et al. (2013), are beneficial for identifying active microbial communities because single-stranded RNA rapidly degrades and is only synthesized by active cells (Hirsch et al., 2010). Organisms from the orders *Methanomicrobiales* and *Methanosarcinales* are known to produce methane through the reduction of CO_2 and methyl group reduction, respectively. Based on the data from the vertical core profiles, it is likely that one or both of these pathways are utilized by methanogens in the RG sediments.

There are two metabolic pathways that may result in the higher than atmospheric concentrations of methane in the subsurface sediments; acetogenic and hydrogenotrophic (equations 4.1 and 4.2).

(Eq 4.1) $CH_3COOH \rightarrow CH_4 + CO_2$

(Eq 4.2) $CO_2 + 4H_2 \rightarrow CH_4 + 2H_2O$

Both pathways result in the production of methane and are preceded by other biological reactions (see Figure 4.1).

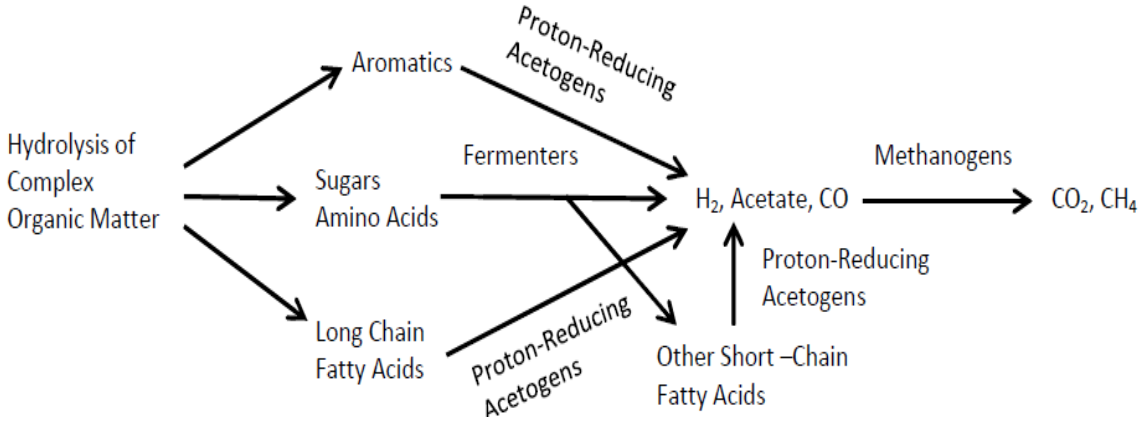

Figure 4.1. The multiple metabolic pathways that result in production in H_2, acetate, and, via methanogenesis, CO_2 and CH_4. Complex organic molecules are hydrolyzed and fermented prior to methanogenesis. CO may also be reduced to methane (Thauer, 1998). Image adapted from Lovley and Chapelle (1995).

Complex organic molecules cannot be directly utilized by methanogens, however, the degradation of such molecules by other microbes could result in production of CO_2, H_2 or simple organic molecules (i.e. acetate) which may be used by methanogens (Madigan et. al., 2003). There is a strong positive linear correlation between carbon dioxide and methane in the 2011 cores which would suggest CO_2 is being produced along with methane such as would result through acetate fermentation (equation 4.1). However, there are other pathways both abiotic and biotic that would result in CO_2 production. The organic carbon in the sediments could be hydrolyzed to volatile fatty acids which may further be fermented or syntrophically reduced to simple carbon compounds (i.e. acetate) which may be utilized by methanogens (see Figure 4.1). Also, previous incubation experiments at 4^oC using glacial sediments from a similar glacial catchment have found an increase in acetate during the microbial reduction of ferric iron (Montross et al., 2013)

and iron reducing microorganisms have been documented in the RG sediments (Mitchell et al., 2013).

If methanogenesis were occurring via CO_2 reduction, H_2 would decrease in concentration with increasing methane concentrations. However, H_2 levels must remain above a threshold concentration to be utilized by methanogens, 0.01-0.07 nmol cm^{-3} (Conrad, 1996). Below the H_2 threshold, methanogens may be outcompeted by other microbes (i.e. homoacetogens) and the H_2 threshold increases with decreasing temperature, particularly below 15°C (Kotsyurbenko, 2005). Reported H_2 concentrations in the vertical sediment profiles were at least twice the threshold concentration suggested by Conrad (1996) indicating that hydrogen availability would not be limiting. Carbon dioxide required for the reaction (equation 4.2) is in abundance and should not limit the reaction. CO, an intermediate in some microbial metabolic pathways (Conrad, 1996; Thauer, 1998), may also be utilized by methanogens as either a carbon source (Thauer, 1998) or an electron source in the absence of H_2 (Madigan et al., 2003). In none of the four cores was CO measured any closer to the surface than 4 cm. The absence of CO in the uppermost portion of the sediment profile may be due to oxic conditions near the surface as the rate of aerobic CO microbial utilization is four times greater than anaerobic utilization (Funk, 1994).

It is also important to consider potential abiotic sources of the methane gas. Two bedrock formations, the Palliser Formation and Mount Hawk Formation, in the RG catchment have been acknowledged as reservoirs for oil and gas (Monahan, 2000). While these formations may potentially contain natural gas (i.e. methane) which may

seep to the surface through fracture systems (Etiope et al., 2013), the methane flux spatial variability at RG forefield is not similar to natural, focused geologic fault or fracture seepage. Also, the high variability of methane fluxes at individual sampling locations and changing methane concentrations within core profiles is not indicative of a steady source. Isotopic analysis of both the $\delta^{13}C_{CH4}$ and δD_{CH4} would aid in discriminating the source of methane as geologic or microbial (Whiticar et al., 1986).

Production of subsurface CO abiotically through chemical oxidation of organic carbon has been demonstrated in a variety of soil types (Conrad, 1996; Conrad and Seller, 1985; Godde et al., 2000), however, this process has not yet been investigated in glacial sediments. Autoxidation of phenolic compounds has been implicated in the abiotic production of CO (Conrad and Seller, 1985) where photo oxidation, the typical pathway of abiotic CO production (Zuo and Jones, 1996), is inhibited by absence of light. The net efflux of CO from sediments will depend on a) the rate of abiotic production b) rate of biotic production and c) subsequent consumption via microbial activity.

The underlying bedrock at RG is largely comprised of impure limestone providing the calcium carbonate source which may result in the abiotic production of carbon dioxide through carbonate dissolution reactions.

Sediments and soils are generally considered a sink for hydrogen gas due to microbial activity therein (Ehhalt and Rohrer, 2009; Godde et al., 2000) except during the fixation of nitrogen (Godde et al., 2000). Chemical reactions have been proposed that may result in elemental hydrogen (Conrad, 1996), the most likely of which being the breaking of silicate bonds resulting in Si and SiO radicals that react with H_2O forming

SiOH and H_2 (Kita et al., 1982). This has been demonstrated (at temperatures ranging from 20-200^oC (Kita et al., 1982)) with rock crushing where fresh mineral surfaces are exposed such as may be found in the freshly comminuted debris from glacial erosional activity and silicates (quartz) are a primary mineral in the sediments at Robertson Glacier (Griggs, 2013).

The reported values of all the gas analytes are greater than atmospheric concentrations; therefore there is an implied source of the gases in the recently exposed subglacial sediments which may be the result of abiotic chemical reactions and/or microbiological processes. While there are some correlations between gas analytes in an individual core, the relationships are not consistent across all the analyzed cores. Such inconsistency may reflect microsite (an environment or location where biological processes differ from those occurring in the whole) microbial activity as acknowledged in other, similarly oligotrophic systems such as the deep marine environment Hydrate Ridge in the Pacific Ocean. Here there is a "periodic infusion" of oxidizing and reducing agents which facilitate the rate of microbial methane production (Colwell et al., 2008). Likewise, in arid sediments that alternate from oxic to anoxic conditions with local hydrologic dynamics, microsite methane production was also demonstrated in what would otherwise be considered an oxic environment (Angel et al., 2011).

4.3 Diffusivity of Methane, CO and CO_2 Gas Through Vertical Core Profile

The sediment cores collected in the proglacial area of Robertson Glacier reveal CH_4 concentrations in the sediments higher than global atmospheric concentrations of

1.79 ppmv (Dlugokencky et al., 2011) or ambient atmospheric concentrations measured at Robertson Glacier (1.81 ppmv). Zones of production and/or consumption of CH_4 within the sediment profile are inferred by the absence of a simple diffusion gradient from depth to the surface, assuming a constant rate of diffusion. Effective diffusion, however, must be considered in terms of sediment characteristics including sediment porosity and water saturation. While the measured porosity of the sediments tends to vary little within the cores the water saturation will vary as the hydrologic dynamics change over the melt season. The rate of gas diffusion in sediments is not constant with depth and depends on the water filled vs. air filled porosity (Kruse et al., 1996). The effective diffusivity of gas will increase with the total porosity but is inhibited as the water filled porosity increases (Figure 3.5). Both of these variables, total and water filled porosity, will affect the flux of gas through the sediments.

The highest methane concentrations were found within 4 cm of the sediment surface. Additionally, there is a peak in methane concentration at 12 cm in core C and methane doubles in concentration between 9 and 6 cm in core A; methane also peaks at 18 cm below the surface in core D. These methane peaks within the core profiles indicate a methane source at the measured depth. Based on the effective diffusive fluxes, the methane flux from 4 cm below the sediment surface to air are, at their maximum, up to 4 orders of magnitude larger than the fluxes derived from the surface GFCs (see Table 3.4). Only once the water saturation is > 90% do the diffusive flux values resemble those of the GFCs. This would indicate that the sediments in the proglacial area of RG are largely water saturated which constrains the subsurface efflux of methane. There is a

methane source at depth within the recently exposed subglacial sediments at RG whose magnitude of flux is under constraint by, at a minimum, physical parameters such as sediment water saturation and, potentially, microbiologic activity.

4.4 Comparison of RG CH_4 Fluxes to Those of Other Glaciated Environments

Similar fluxes of methane have been measured in other comparable environments, (i.e. Mittivakkat Glacier in Greenland (Barcena et al., 2010) and the Swiss Alps (Nauer et al., 2012a)). These studies also pointed to the existence of a microbial source at depth (see Figure 4.2). Barcena et al. (2010) deployed 12 gas flux chambers across the proglacial area at Mittivakkat Glacier in Greenland. The only GFC demonstrating a net efflux of methane to the atmosphere was within 1 m of the glacier terminus (data presented in Figure 4.2). All other GFCs revealed methane consumption or net influx and ranged from ~ 80 m to 2 km from the glacier terminus. Nauer et al. (2012) conducted 59 soil-gas samplings at 13 glacial forefields, ~100-200 m from the glacier terminus, in the Swiss Alps concluding that the underlying bedrock controls the flux of methane. Calcareous sediments resulted in a net efflux and most sites of siliceous composition resulted in a net influx of methane to sediments, indicating microbial methane consumption. The average efflux data from the 22 sampling locations from glaciated catchments on calcareous substrate is shown in Figure 4.2.

In the three studies compared in Figure 4.2, all reported both negative and positive methane fluxes, indicating both source and sink potential in the proglacial area. However, the previous studies (i.e. Barcena et al., (2010) and Nauer et al., (2012)) used

multiple location, single time point flux measurements. This study concludes that such point measurements may not be representative for determining a net seasonal flux as they do not consider temporal variability. For example, the highest surface to air methane flux measured at RG was 11.0 µmol m^{-2} d^{-1}. If this value were extrapolated as an annual flux from the RG proglacial area, it would overestimate the methane source contribution (3.1 x 10^{-10} Tg yr^{-1}) by two orders of magnitude compared to the melt season average flux (6.2 x 10^{-12} Tg yr^{-1}).

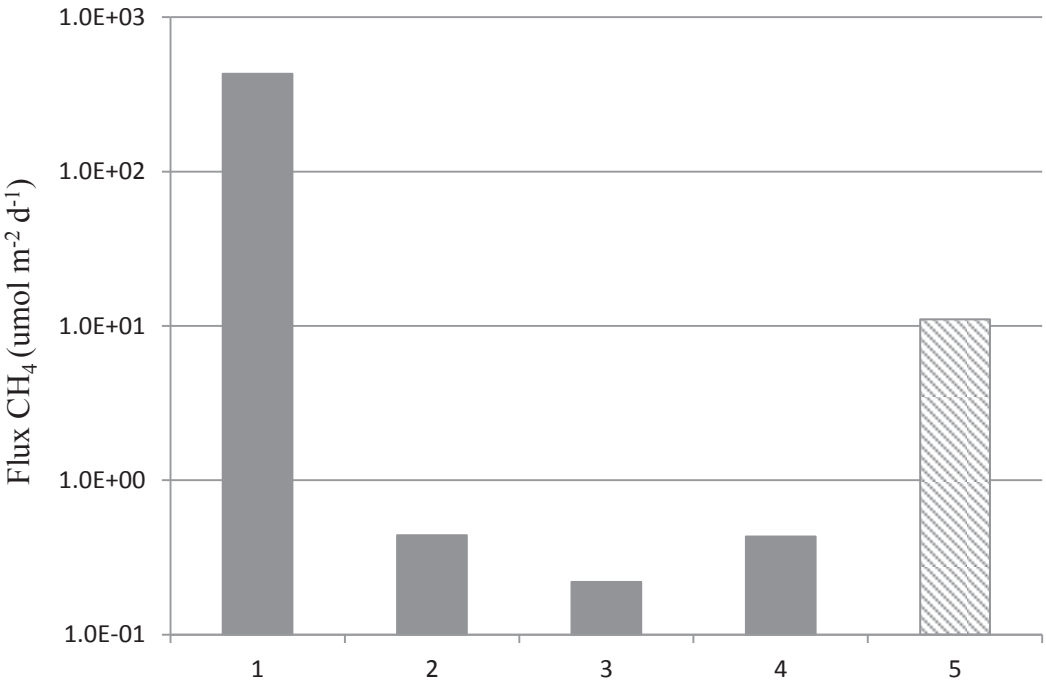

Figure 4.2. Methane fluxes measured in environments comparable to Robertson Glacier (RG). Note the log scale on the y-axis.
[1]Nauer et al. (2012a) proglacial sediments, Swiss Alps.
[2]Barcena et al. (2010) proglacial sediments Mittivakkat Glacier, east Greenland.
[3]RG average surface flux from glacial sediments to the atmosphere.
[4]RG average core diffusive flux, values at 99% water saturation as a minimum flux.
[5]RG maximum surface to air flux measured via the static chamber method.

4.5 Future Research

The physical and biotic processes that affect the flux of methane from RG sediments to the atmosphere are not well understood. Future studies should include 1) measurements of dissolved organic carbon (DOC) which may be involved in production of the gas analytes, 2) analysis of 16S rRNA gene data from sediment cores to correlate gas analytes concentrations with microbial community diversity, 3) isotopic analyses of $\delta^{13}C_{CH4,}$ which may provide a more definitive signature on the methane source, biogenic or geologic, and 4) measurements of the sediment water saturation simultaneous with static chamber measurements to determine a correlation, if any, between methane flux and sediment saturation. These additional analyses may help to better understand the driving forces behind the flux of methane from the glacial sediments at RG.

4.6 Conclusion

The primary objective of this research was to quantify the flux of methane from the glacial sediments at Robertson Glacier assessing its spatial and temporal variability. The average melt season methane flux from the glacial sediments to the atmosphere was 0.15 μmol m^{-2} d^{-1}. There were no correlations between the flux of methane and a) sediment temperature and b) the flux of carbon dioxide and carbon monoxide. Sediments that were further from the glacier terminus and therefore had been exposed to atmospheric conditions longer, demonstrated the lowest flux of methane and were the strongest methane sink (negative flux). Likewise, the sediments in closest proximity to the glacier terminus demonstrated the strongest net efflux of methane. Concentrations of

methane, carbon dioxide, carbon monoxide and hydrogen at depth within sediment core profiles were, when detected, higher than ambient atmospheric concentrations. The core profiles indicate, through gas analyte associations, that methane may be produced biotically through hydrogenotrophic and/or acetogenic pathways. The high concentrations of methane at depth within the sediment profiles and the low average efflux of methane measured at the sediment surface indicate subsurface processes, such as decreased effective diffusivity due water saturation or microbial activity, that impede the flux of methane from depth to the atmosphere.

Past research has cultured methanogens from RG sediments at temperatures down to 4^{o}C and measured methane up to 29 ppmv in RG porewater samples (Boyd et al., 2010). Additionally, methanogenic orders have been identified in RG subglacial sediments (Hamilton et al., 2013) as have biomarkers suggestive of methanogenic activity (Boyd et al., 2010). This research presents direct measurement of a net efflux of methane from the recently exposed subglacial sediments to the atmosphere, higher than atmospheric methane concentrations at depth in the sediments and the presence of substrates which may be utilized by methanogens. The converging lines of evidence, indirect and direct, discussed above indicate a strong likelihood that the source of methane in the sediments at RG is biologic and the result of an active microbial consortium which includes Archaeal methanogens.

REFERENCES CITED

Allan, W., Manning, M. R., Lassey, K. R., Lowe, D. C., and Gomez, A. J., 2001, Modeling the variation of delta C-13 in atmospheric methane: Phase ellipses and the kinetic isotope effect: Global Biogeochemical Cycles, v. 15, no. 2, p. 467-481.

Anderson, S. P., 2007, Biogeochemistry of glacial landscape systems: Annual Review of Earth and Planetary Sciences, v. 35, no. 1, p. 375-399.

Angel, R., Matthies, D., and Conrad, R., 2011, Activation of methanogenesis in arid biological soil crusts despite the presence of oxygen: Plos One, v. 6, no. 5.

Archer, D., 2007, Methane hydrate stability and anthropogenic climate change: Biogeosciences, v. 4, no. 4, p. 521-544.

Aronson, E. L., Allison, S. D., and Helliker, B. R., 2013, Environmental impacts on the diversity of methane-cycling microbes and their resultant function: Frontiers in Microbiology, v. 4, p. 225.

Barcena, T. G., Yde, J. C., and Finster, K. W., 2010, Methane flux and high-affinity methanotrophic diversity along the chronosequence of a receding glacier in Greenland: Annals of Glaciology, v. 51, no. 56, p. 23-31.

Benn, D. I., and Evans, D. J. A., 2010, Glaciers and Glaciation, London, UK, Hodder Arnold Education.

Boyd, E. S., Skidmore, M., Mitchell, A. C., Bakermans, C., and Peters, J. W., 2010, Methanogenesis in subglacial sediments: Environmental Microbiology Reports, v. 2, no. 5, p. 685-692.

Boyd, E. S., Lange, R. K., Mitchell, A. C., Havig, J. R., Hamilton, T. L., Lafreniere, M. J., Shock, E. L., Peters, J. W., and Skidmore, M., 2011, Diversity, abundance, and potential activity of nitrifying and nitrate-reducing microbial assemblages in a subglacial ecosystem: Applied and Environmental Microbiology, v. 77, no. 14, p. 4778-4787.

Breas, O., Guillou, C., Reniero, F., and Wada, E., 2002, The global methane cycle: Isotopes and mixing ratios, sources and sinks: Isotopes in Environmental and Health Studies, v. 37, no. 4, p. 257-379.

Brook, E. J., Harder, S., Severinghaus, J., Steig, E. J., and Sucher, C. M., 2000, On the origin and timing of rapid changes in atmospheric methane during the Last Glacial Period: Global Biogeochemical Cycles, v. 14, no. 2, p. 559-572.

Campen, R. K., Sowers, T., and Alley, R. B., 2003, Evidence of microbial consortia metabolizing within a low-latitude mountain glacier: Geology, v. 31, no. 3, p. 231-234.

Colwell, F. S., Boyd, S., Delwiche, M. E., Reed, D. W., Phelps, T. J., and Newby, D. T., 2008, Estimates of biogenic methane production rates in deep marine sediments at Hydrate Ridge, Cascadia margin: Applied and Environmental Microbiology, v. 74, no. 11, p. 3444-3452.

Conrad, R., and Seller, W., 1985, Characteristics of abiological carbon monoxide formation from soil organic matter, humic acids, and phenolic compounds: Environmental Science & Technology, v. 19, no. 12, p. 1165-1169.

Conrad, R., 1995, Soil microbial processes and the cycling of atmospheric trace gases: Philosophical Transactions of the Royal Society of London Series a-Mathematical Physical and Engineering Sciences, v. 351, no. 1696, p. 219-230.

Conrad, R., 1996, Soil microorganisms as controllers of atmospheric trace gases (H_2, CO, CH_4, OCS, N_2O, and NO): Microbiological Reviews, v. 60, no. 4, p. 609-640.

Conrad, R., 2009, The global methane cycle: recent advances in understanding the microbial processes involved: Environmental Microbiology Reports, v. 1, no. 5, p. 285-292.

Dlugokencky, E. J., Nisbet, E. G., Fisher, R., and Lowry, D., 2011, Global atmospheric methane: budget, changes and dangers: Philosophical Transactions of the Royal Society a-Mathematical Physical and Engineering Sciences, v. 369, no. 1943, p. 2058-2072.

Dyke, A. S., Andrews, J. T., Clark, P. U., England, J. H., Miller, G. H., Shaw, J., and Veillette, J. J., 2002, The Laurentide and Innuitian ice sheets during the Last Glacial Maximum: Quaternary Science Reviews, v. 21, no. 1-3, p. 9-31.

Ehhalt, D. H., and Rohrer, F., 2009, The tropospheric cycle of H_2: A critical review: Tellus Series B-Chemical and Physical Meteorology, v. 61, no. 3, p. 500-535.

Ehrlich, H. L., 1998, Geomicrobiology: Its significance for geology: Earth-Science Reviews, v. 45, no. 1-2, p. 45-60.

Etiope, G., Drobniak, A., and Schimmelmann, A., 2013, Natural seepage of shale gas and the origin of "eternal flames" in the Northern Appalachian Basin, USA: Marine and Petroleum Geology, v. 43, p. 178-186.

Foght, J., Aislabie, J., Turner, S., Brown, C. E., Ryburn, J., Saul, D. J., and Lawson, W., 2004, Culturable bacteria in subglacial sediments and ice from two Southern Hemisphere glaciers: Microbial Ecology, v. 47, no. 4, p. 329-340.

Funk, D. W., Pullman, E. R, Peterson, K. M., 1994, Influence of water table on carbon dioxide, carbon monoxide, and methane fluxes from taiga bog microcosms: Global Biogeochemical Cycles, v. 8, no. 3, p. 271-278.

Godde, R., Meuser, K., and Conrad, R., 2000, Hydrogen consumption and carbon monoxide production in soils with different properties: Biology and Fertility of Soils, v. 32, no. 2, p. 129-134.

Griggs, R., 2013, Characterization of subglacial till from Robertson Glacier, Alberta, Canada. Masters Thesis. Montana State University, Department of Earth Science.

Hamilton, T. L., Peters, J. W., Skidmore, M. L., and Boyd, E. S., 2013, Molecular evidence for an active endogenous microbiome beneath glacial ice: ISME Journal, v. 7, no. 7, p. 1402-1412.

Heiri, O., Lotter, A. F., and Lemcke, G., 2001, Loss on ignition as a method for estimating organic and carbonate content in sediments: reproducibility and comparability of results: Journal of Paleolimnology, v. 25, no. 1, p. 101-110.

Hirsch, P. R., Mauchline, T. H., and Clark, I. M., 2010, Culture-independent molecular techniques for soil microbial ecology: Soil Biology and Biochemistry, v. 42, no. 6, p. 878-887.

Hoehler, T. M., Alperin, M. J., Albert, D. B., and Martens, C. S., 1994, Field and laboratory studies of methane oxidation in an anoxic marine sediment-Evidence for a methanogen-sulfate reducer consortium: Global Biogeochemical Cycles, v. 8, no. 4, p. 451-463.

IPCC (Intergovernmental Panel on Climate Change), 2007, Climate Change 2007: The Physical Science Basis, Cambridge, United Kingdom and New York, NY, USA, Cambridge University Press, 996 p.

Kirschivink, J. L., 1992, Late Proterozoic low-latitude global glaciation: The snowball Earth, *in* Klein, J. W. S. a. C., ed., The Proterozoic Biosphere: A Multidisciplinary Study., Cambridge University Press, p. 51-52.

Kita, I., Matsuo, S., and Wakita, H., 1982, H_2 generation by reaction between H_2O and crushed rock: An experimental study on H_2 degassing from the active fault zone: Journal of Geophysical Research, v. 87, no. B13, p. 10789.

Knittel, K., and Boetius, A., 2009, Anaerobic oxidation of methane: Progress with an unknown process: Annual Review of Microbiology, v. 63, p. 311-334.

Kotsyurbenko, O. R., Chin, K. J., Glagolev, M. V., Stubner, S., Simankova, M. V., Nozhevnikova, A. N., and Conrad, R., 2004, Acetoclastic and hydrogenotrophic methane production and methanogenic populations in an acidic West-Siberian peat bog: Environmental Microbiology, v. 6, no. 11, p. 1159-1173.

Kotsyurbenko, O. R., 2005, Trophic interactions in the methanogenic microbial community of low-temperature terrestrial ecosystems: FEMS Microbiology Ecology, v. 53, no. 1, p. 3-13.

Kruse, C. W., Moldrup, P., and Iversen, N., 1996, Modeling diffusion and reaction in soils: II. Atmospheric methane diffusion and consumption in a forest soil: Soil Science, v. 161, no. 6, p. 355-365.

LI-COR, 2012, LI-8100A automated soil CO_2 flux system; Survey, long-term and multiplexed measurements.

Lovley, D. R., and Chapelle, F. H., 1995, Deep subsurface microbial processes: Reviews of Geophysics, v. 33, no. 3, p. 365-381.

Madigan, M. T., Martinko, J. M., and Parker, J., 2003, Brock Biology of Microorganisms, Upper Saddle River, NJ, Prentice Hall/Pearson Education.

Manger, G. E., 1963, Porosity and Bulk Density of Sedimentary Rocks, Geological Survey Bulletin 1144-E, United States Government Printing Office, Washington.

McMechan, M. E., 1998, Geology of Peter Lougheed Provincial Park, Rocky Mountain Front Ranges, Alberta. Open File Report 2057. Alberta, Canada: Geological Survey of Canada.

Melton, J. R., Whiticar, M. J., and Eby, P., 2011, Stable carbon isotope ratio analyses on trace methane from ice samples: Chemical Geology, v. 288, no. 3-4, p. 88-96.

Mitchell, A. C., Lafreniere, M. J., Skidmore, M. L., and Boyd, E. S., 2013, Influence of bedrock mineral composition on microbial diversity in a subglacial environment: Geology, v. 41, no. 8, p. 855-858.

Moldrup, P., Olesen, T., Komatsu, T., Schjonning, P., and Rolston, D. E., 2001, Tortuosity, diffusivity, and permeability in the soil liquid and gaseous phases: Soil Science Society of America Journal, v. 65, no. 3, p. 613-623.

Monahan, P. A., 2000, The geology and oil and gas potential of the Fernie-Elk Valley Area, Southeastern British Columbia: Petroleum Geology Special Paper 2000-1, p. 56.

Montross, S. N., 2007, Geochemical evidence for microbially mediated subglacial mineral weathering. Masters Thesis. Montana State University, Department of Earth Science.

Montross, S. N., Skidmore, M., Tranter, M., Kivimaki, A. L., and Parkes, R. J., 2013, A microbial driver of chemical weathering in glaciated systems: Geology, v. 41, no. 2, p. 215-218.

Nauer, P. A., Dam, B., Liesack, W., Zeyer, J., and Schroth, M. H., 2012, Activity and diversity of methane-oxidizing bacteria in glacier forefields on siliceous and calcareous bedrock: Biogeosciences, v. 9, no. 6, p. 2259-2274.

Parkin, T. B., and Venterea, R. T., 2010, Sampling Protocols. Chapter 3. Chamber-Based Trace Gas Flux Measurements, Beltsville, MD, Sampling Protocols.

Raynaud, D., Barnola, J. M., Chappellaz, J., Zardini, D., Jouzel, J., and Lorius, C., 1992, Glacial interglacial evolution of greenhouse gases as inferred from ice core analysis- A review of recent results: Quaternary Science Reviews, v. 11, no. 4, p. 381-386.

Reeburgh, W. S., 2007, Oceanic methane biogeochemistry: Chemical Reviews, v. 107, no. 2, p. 486-513.

Scanlon, B. R., Nicot, J. P., and Massman, J. W., 2001, Soil Physics Companion, CRC Press.

Schoell, M., 1988, Multiple origins of methane in the Earth: Chemical Geology, v. 71, no. 1-3, p. 1-10.

Shakhova, N., Semiletov, I., Leifer, I., Salyuk, A., Rekant, P., and Kosmach, D., 2010, Geochemical and geophysical evidence of methane release over the East Siberian Arctic Shelf: Journal of Geophysical Research, v. 115, no. C8.

Sharp, M., Parkes, J., Cragg, B., Fairchild, I. J., Lamb, H., and Tranter, M., 1999, Widespread bacterial populations at glacier beds and their relationship to rock weathering and carbon cycling: Geology, v. 27, no. 2, p. 107-110.

Sharp, M., Creaser, R. A., and Skidmore, M., 2002, Strontium isotope composition of runoff from a glaciated carbonate terrain: Geochimica et Cosmochimica Acta, v. 66, no. 4, p. 595-614.

Skidmore, M. L., Foght, J. M., and Sharp, M. J., 2000, Microbial life beneath a high Arctic glacier: Applied and Environmental Microbiology, v. 66, no. 8, p. 3214-3220.

Skidmore, M., Anderson, S. P., Sharp, M., Foght, J., and Lanoil, B. D., 2005, Comparison of microbial community compositions of two subglacial environments reveals a possible role for microbes in chemical weathering processes: Applied and Environmental Microbiology, v. 71, no. 11, p. 6986-6997.

Souchez, R., Jouzel, J., Landais, A., Chappellaz, J., Lorrain, R., and Tison, J. L., 2006, Gas isotopes in ice reveal a vegetated central Greenland during ice sheet invasion: Geophysical Research Letters, v. 33, no. 24.

Stauffer, B., 2000, Long term climate records from polar ice: Space Science Reviews, v. 94, no. 1-2, p. 321-336.

Stibal, M., Wadham, J. L., Lis, G. P., Telling, J., Pancost, R. D., Dubnick, A., Sharp, M. J., Lawson, E. C., Butler, C. E. H., Hasan, F., Tranter, M., and Anesio, A. M., 2012, Methanogenic potential of Arctic and Antarctic subglacial environments with contrasting organic carbon sources: Global Change Biology, v. 18, no. 11, p. 3332-3345.

Thauer, R. K., 1998, Biochemistry of methanogenesis: A tribute to Marjory Stephenson: Microbiology-UK, v. 144, p. 2377-2406.

Tranter, M., Sharp, M. J., Lamb, H. R., Brown, G. H., Hubbard, B. P., and Willis, I. C., 2002, Geochemical weathering at the bed of Haut Glacier d'Arolla, Switzerland - a new model: Hydrological Processes, v. 16, no. 5, p. 959-993.

Tranter, M., Skidmore, M., and Wadham, J., 2005, Hydrological controls on microbial communities in subglacial environments: Hydrological Processes, v. 19, no. 4, p. 995-998.

Tucker, W. A., and Nelken, L. H., 1982, Diffusion coefficients in air and water, *in* Lyman, W. J., Reehl, W. F., and Rosenblatt, D. H., eds., Handbook of Chemical Property Estimation Methods: Environmental Behavior of Organic Compounds, American Chemical Society.

Wadham, J. L., Tranter, M., Tulaczyk, S., and Sharp, M., 2008, Subglacial methanogenesis: A potential climatic amplifier?: Global Biogeochemical Cycles, v. 22, no. 2.

Wadham, J. L., Arndt, S., Tulaczyk, S., Stibal, M., Tranter, M., Telling, J., Lis, G. P., Lawson, E., Ridgwell, A., Dubnick, A., Sharp, M. J., Anesio, A. M., and Butler, C. E. H., 2012, Potential methane reservoirs beneath Antarctica: Nature, v. 488, no. 7413, p. 633-637.

Wagner, D., Lipski, A., Embacher, A., and Gattinger, A., 2005, Methane fluxes in permafrost habitats of the Lena Delta: Effects of microbial community structure and organic matter quality: Environmental Microbiology, v. 7, no. 10, p. 1582-1592.

Wagner, S. W., Reicosky, D. C., and Alessi, R. S., 1997, Regression models for calculating gas fluxes measured with a closed chamber: Agronomy Journal, v. 89, no. 2, p. 279-284.

Walter, K. M., Zimov, S. A., Chanton, J. P., Verbyla, D., and Chapin, F. S., 3rd, 2006, Methane bubbling from Siberian thaw lakes as a positive feedback to climate warming: Nature, v. 443, no. 7107, p. 71-75.

Weisenberg, D. A., and Guinasso, N. L. J., 1979, Equilibrium solubilities of methane, carbon monoxide, and hydrogen in water and sea water: Journal of Chemical and Engineering Data, v. 24, no. 4, p. 356-360.

Weiss, R. F., 1974, Carbon dioxide in water and seawater: The solubility of a non-ideal gas: Marine Chemistry, v. 2, no. 3, p. 203-215.

Weitemeyer, K. A., and Buffett, B. A., 2006, Accumulation and release of methane from clathrates below the Laurentide and Cordilleran ice sheets: Global and Planetary Change, v. 53, no. 3, p. 176-187.

Whiticar, M. J., Faber, E., and Schoell, M., 1986, Biogenic methane formation in marine and fresh-water environments: CO_2 reduction vs acetate fermentation isotope evidence Geochimica et Cosmochimica Acta, v. 50, no. 5, p. 693-709.

Whiticar, M., and Schaefer, H., 2007, Constraining past global tropospheric methane budgets with carbon and hydrogen isotope ratios in ice: Philosophical Transactions of the Royal Society a-Mathematical Physical and Engineering Sciences, v. 365, no. 1856, p. 1793-1828.

Wolff, E., and Spahni, R., 2007, Methane and nitrous oxide in the ice core record: Philosophical Transactions of the Royal Society a-Mathematical Physical and Engineering Sciences, v. 365, no. 1856, p. 1775-1792.

Zuo, Y., and Jones, R. D., 1996, Photochemical production of carbon monoxide in authentic rainwater: Geophysical Research Letters, v. 23, no. 20, p. 2769-2772.

APPENDICES

APPENDIX A

GAS CHROMATOGRAPH SCHEMATIC

Gas Chromatograph (SRI 8610C) Configuration

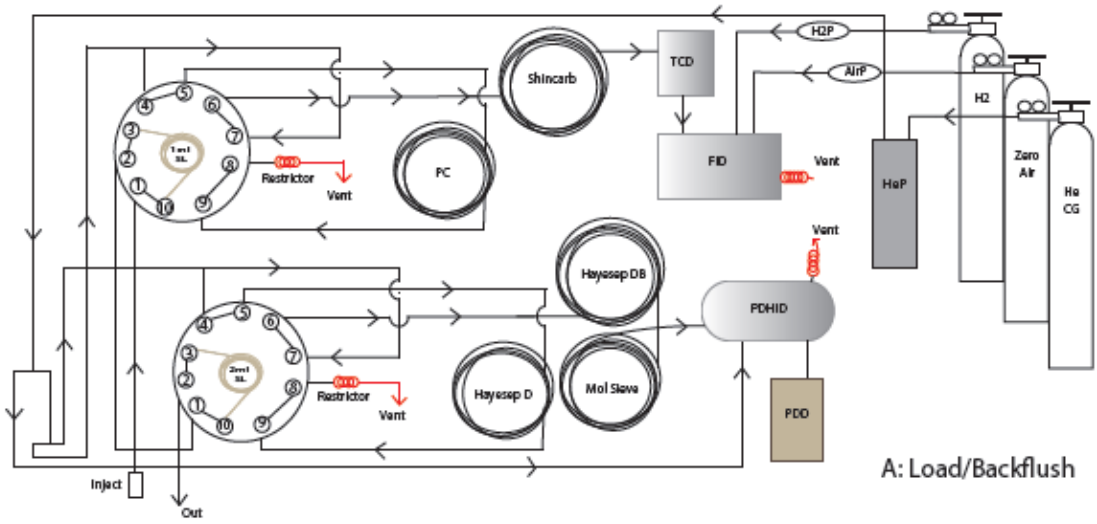

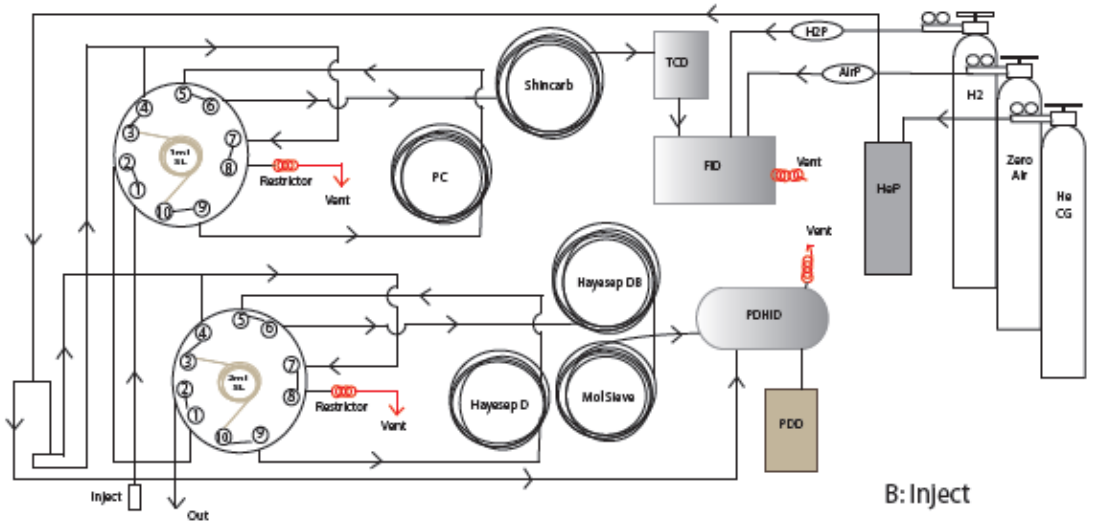

Key:

SL=sample loop
PC=precolumn
TCD= thermal conductivity detector
FID=flame ionization detector
H2P= hydrogen purifier
AirP=air purifier
HeP=helium purifier
H2=hydrogen tank
Zero Air=air tank
HeCG=helium carrier gas
PDD=pulsed discharge detector
PDHID=pulsed discharge helium ionization detector

APPENDIX B

CH_4, CO_2 and CO FLUX VALUES

Table B.1. Methane flux values from all GFCs sampled during 2012 field season. No data (n/d) denotes flux values that were not included due to systematic errors, GFC perturbations or T_o headspace values were outside 10% of the RG average atmospheric concentration of 1.81 ppmv. D1, D2 and D3 are the depth chambers at 5, 10 and 15 cm, respectively.

		GFC									
SP	**Dates**	**1**	**2**	**3**	**4**	**5**	**6**	**7**	**D1**	**D2**	**D3**
1	28-30 July	11.02	1.21	n/d	-0.58	0.70	0.27	3.67	0.45	0.85	0.32
2	2-4 Aug	n/d	-1.68	n/d	-1.53	0.49	-0.23	0.02	0.12	-0.56	2.05
3	7-8 Aug	0.02	-0.30	n/d	-0.37	-0.30	-0.02	-0.34	-1.28	-2.37	-0.56
4	11-13 Aug	2.01	-1.36	1.37	1.64	-1.27	-1.90	0.06	-5.92	-0.57	n/d
5	17- 19 Aug	n/d	n/d	0.08	n/d	n/d	-0.20	n/d	n/d	0.88	-2.10
6	25-27 Aug	-1.02	-1.33	0.02	2.58	-2.21	-0.18	0.02	0.41	-0.16	-0.53
7	1-3 Sept	0.51	1.17	0.60	n/d	-1.88	-3.08	-0.43	3.97	4.13	n/d
8	7-9 Sept	1.04	-0.31	-0.14	4.28	0.04	0.66	-0.16	6.09	2.64	-0.08
9	13-14 Sept	n/d	0.39	0.86	0.43	n/d	n/d	0.35	-4.78	n/d	1.90
10	20-22 Sept	n/d	-2.40	-0.35	n/d	-0.30	n/d	0.14	n/d	n/d	6.41

Table B.2. Carbon dioxide flux values from all GFCs sampled during 2012 field season. No data (n/d) denotes flux values that were not included due to systematic errors, GFC perturbations or T_o headspace values were outside 6% of the RG atmospheric concentration measured the same day (actual values will vary by day). D1, D2 and D3 are the depth chambers at 5, 10 and 15 cm, respectively.

		GFC									
SP	**Dates**	**1**	**2**	**3**	**4**	**5**	**6**	**7**	**D1**	**D2**	**D3**
1	28-30 July	-242.2	-297.9	n/d	n/d	-100.0	38.0	-203.8	126.5	528.3	56.7
2	2-4 Aug	205.8	100.7	n/d	125.5	n/d	-390.8	-301.7	-457.9	-296.4	-67.2
3	7-8 Aug	129.7	40.3	n/d	-17.7	n/d	112.7	37.2	464.5	99.8	-94.3
4	11-13 Aug	223.3	-92.4	n/d	65.6	-10.7	125.7	277.9	507.7	456.4	156.6
5	17- 19 Aug	63.7	-230.1	257.7	628.2	278.9	-44.5	3.9	-180.4	215.0	217.9
6	25-27 Aug	32.5	-395.2	n/d	n/d	n/d	73.3	n/d	402.2	62.0	1384.6
7	1-3 Sept	46.4	-0.6	115.6	-121.9	431.7	360.8	60.8	428.5	484.8	633.7
8	7-9 Sept	114.8	-165.7	-193.7	-168.6	-426.7	32.6	135.6	-823.6	-801.4	20.4
9	13-14 Sept	110.6	93.9	-312.4	-144.7	n/d	149.7	103.7	12.0	-359.1	224.9
10	20-22 Sept	137.6	187.2	180.9	-104.4	-166.4	69.1	474.1	290.4	-336.3	1654.1

Table B.3. Carbon monoxide flux values from all GFCs sampled during 2012 field season. No data (n/d) denotes flux values that were not included due to systematic errors, GFC perturbations or T_o headspace values were outside 200% (see discussion in section 2.2.6) of the RG atmospheric concentrations measured (monthly values were July: 0.77 ppmv, August: 0.89 ppmv, September 1-21: 0.91 ppmv, and September 22nd: 3.24 ppmv). D1, D2 and D3 are the depth chambers at 5, 10 and 15 cm, respectively.

		GFC									
SP	**Dates**	**1**	**2**	**3**	**4**	**5**	**6**	**7**	**D1**	**D2**	**D3**
1	28-30 July	27.41	31.81	n/d	9.99	24.72	11.73	27.22	8.47	62.17	-8.14
2	2-4 Aug	3.47	-7.32	n/d	-12.34	-8.89	-4.59	2.73	25.28	n/d	-6.64
3	7-8 Aug	n/d	4.04	n/d	-5.21	-10.32	14.50	n/d	n/d	5.91	8.07
4	11-13 Aug	7.18	n/d	-2.42	-10.40	46.78	2.31	19.67	n/d	n/d	n/d
5	17- 19 Aug	n/d	n/d	0.00	55.03	65.33	n/d	-10.00	n/d	n/d	n/d
6	25-27 Aug	29.33	n/d	n/d	n/d	n/d	n/d	19.08	-15.01	n/d	-41.11
7	1-3 Sept	3.35	0.57	-1.81	n/d	-1.11	6.93	5.27	-25.18	24.48	19.89
8	7-9 Sept	5.87	10.36	17.67	13.24	29.03	18.98	-1.92	49.68	33.41	-2.19
9	13-14 Sept	n/d	n/d	n/d	n/d	n/d	n/d	n/d	118.28	n/d	n/d
10	20-22 Sept	23.13	25.99	22.23	42.97	12.90	-7.48	n/d	n/d	191.56	-42.04